Distribution and activation of melanin-concentrating hormone receptor-1 at dopaminergic, GABAergic, and glutamatergic neurons in the ventral tegmental area

by

Duncan Spencer

A thesis submitted to the Faculty of Graduate and Postdoctoral Affairs

in partial fulfillment of the requirements of the degree of

Master of Science

in

Neuroscience

Department of Neuroscience

Carleton University

Ottawa, Ontario, Canada

Abstract

Melanin-concentrating hormone (MCH) is an orexigenic neuropeptide that acts through its receptor (MCHR1) to promote positive energy balance by increasing food intake and decreasing energy expenditure. MCH has been shown to inhibit dopamine release from the mesocorticolimbic dopamine pathway originating in the ventral tegmental area (VTA), and a hyperdopaminergic state underlies hyperactivity observed in animals lacking MCH or MCHR1. However, it is not known if the inhibitory effect of MCH on dopaminergic tone could be due to direct regulation of dopaminergic VTA neurons. We used a combination of molecular, neuroanatomical, and electrophysiological techniques to assess MCHR1 expression and activation in the VTA. MCH neurons project to the VTA, which comprises nerve terminals that contain MCH and may represent MCH release sites. Consistent with this, we detected MCHR1 expression on major VTA cell types, including those that are dopaminergic, GABAergic, and glutamatergic. Functional MCHR1 activation may regulate dopamine release via two mechanisms, one by acutely and directly inhibiting dopaminergic VTA neurons, and the other by disinhibiting glutamatergic afferents to dopaminergic VTA neurons. While we have not measured dopamine release in this present thesis, we postulate that MCH may acutely suppress dopamine release, while concurrently engaging local glutamatergic signaling to restore dopamine levels. These results signify that the VTA is a novel target for MCH-mediated physiology, including for the maintenance of energy homeostasis.

Acknowledgements

I would like to thank my supervisor, Dr. Melissa Chee, for all her support, guidance, and insight over the course of my studies at Carleton.

I would also like to thank Dr. Alfonso Abizaid, Dr. Shawn Hayley, Dr. Iain McKinnell, and Dr. Hongyu Sun, for serving as my committee and offering their time, advice, and support.

I would like to thank all the current and past members of the Chee lab (Cheetos) for all their help and for making lab all the more enjoyable. Special thanks to Ralitsa Nikolova for her help analyzing ISH signal, Mikayla Payant for helping with anterograde injection studies, and Jesukhogie Williams-Ikhenoba for his help with gene and protein expression studies. Additional thanks to Bianca Bono for helping to prepare tissue and establish a combined ISH and IHC protocol.

Thank you to the Mighty 93.1, CKCU FM, for always having fantastic programming to listen to and for allowing me to host my own show “Track 11“ (https://cod.ckcufm.com/programs/518/info.html).

Last but not least, I would also like to thank Kirk Spencer, Karen Roberts, Simon Spencer, Peter Roberts, Thelma Gowing, and Ava Sotoudehrad for all their love and support over the course of my studies.

Table of Contents

List of Abbreviations

ACSF	Artificial cerebrospinal fluid
ANOVA	Analysis of variance
AP	Anteroposterior
ARA	Allen reference atlas
Arc	Arcuate nucleus of the hypothalamus
CB	Continuous band
cDNA	Complementary deoxyribonucleic acid
DA	Dopamine
DAT	Dopamine transporter
DI	Distilled
DNA	Deoxyribonucleic acid
DV	Dorsoventral
EGFP	Enhanced green fluorescent protein
ERKs	Extracellular signal-regulated kinases
EYFP	Enhanced yellow fluorescent protein
GABA	Gamma-aminobutyric acid
GAD	Glutamate decarboxylase
Gapdh	Glyceraldehyde-3-phosphate dehydrogenase
GPCR	G-protein coupled receptor
IHC	Immunohistochemistry
ISH	*In situ* hybridization
LHA	Lateral hypothalamic area
LUTs	Look up table values
MCH	Melanin-concentrating hormone
MCH-ir	Melanin-concentrating hormone immunoreactivity
Mch-KO	Melanin-concentrating hormone knock-out
MCHR1	Melanin-concentrating hormone receptor 1
Mchr1-KO	Melanin-concentrating hormone receptor 1 knock-out
MCHR2	Melanin-concentrating hormone receptor 2
ML	Mediolateral
mRNA	Messenger ribonucleic acid
NAcc	Nucleus accumbens
NDS	Normal donkey serum
NPY	Neuropeptide Y
PBS	Phosphate buffered saline
PBT	Phosphate buffered saline solution with 0.3% triton
POMC	Proopiomelanocortin
PPIB	Peptidyl-prolyl cis-trans isomerase B
RMP	Resting membrane potential
RNA	Ribonucleic acid
RT	Room temperature
RT-PCR	Reverse transcription polymerase chain reaction
sEPSC	Spontaneous excitatory postsynaptic current
sIPSC	Spontaneous inhibitory postsynaptic current
TH	Tyrosine hydroxylase
TTX	Tetrodotoxin
tVTA	Tail of the ventral tegmental area
Vgat	Vesicular GABA transporter
Vglut2	Vesicular glutamate transporter 2
VMAT	Vesicular monoamine transporter
VTA	Ventral tegmental area
WT	Wildtype

1. Introduction

Neurons expressing melanin-concentrating hormone (MCH) are largely restricted to the lateral hypothalamus but they have widespread projections throughout the brain (**Section 1.1**) and are implicated in diverse functions. The best-defined role of MCH is its contribution to the regulation of feeding and energy balance (Diniz & Bittencourt, 2017; Qu et al., 1996). Intracerebroventricular administration of MCH promotes food intake (Qu et al., 1996; Rossi et al., 1997; Tritos et al., 1998), and MCH expression in the lateral hypothalamic area (LHA) is upregulated during periods of fasting to promote food intake (Qu et al., 1996). Furthermore, chronic MCH administration leads to increased body weight and the development of diet-induced obesity (Della-Zuana et al., 2002; Gomori et al., 2002; Shearman et al., 2003). Much insight underlying the actions of MCH that promotes positive energy balance were gained through transgenic models of MCH or MCH receptor (MCHR1) mouse models (**Section 1.2**). Feeding incorporates both homeostatic and hedonic elements, with motivation underlying food seeking and preference (Pissios et al., 2008; Saper et al., 2002). Interestingly, there is evidence suggesting the dopaminergic system, implicated in the regulation of reward and motivation (Berridge, 2007; Bromberg-Martin et al., 2010; Wise, 2004), as a point of convergence for MCH action and may be important for integrating feeding and reward pathways (**Section 1.3**). In particular, this thesis will focus on the integration of MCH action within the ventral tegmental area (VTA; **Section 1.4**).

1.1 Anatomical characterization of the MCH System

1.1.1 Distribution of MCH and *Mchr1* mRNA

In the rodent, MCH cell bodies are found exclusively in the LHA and zona incerta (Bittencourt et al., 1992; Croizier et al., 2010). Almost all MCH neurons are glutamatergic (Chee et al., 2015; Schneeberger et al., 2018). They express *Slc17a6* mRNA encoding for vesicular glutamate transporter 2 (*Vglut2*; Chee et al., 2015; Mickelsen et al., 2017; Schneeberger et al., 2018) and can release glutamate (Chee et al., 2015). It has also been suggested MCH neurons may release GABA (Jego et al., 2013), however, expression of *Slc32a1* mRNA encoding the vesicular GABA transporter (*Vgat*) is not observed in MCH neurons (Mickelsen et al., 2017; Schneeberger et al., 2018).

Projections from MCH neurons are widely distributed throughout the brain with high to moderate MCH-immunoreactivity (MCH-ir) observed in the medial and lateral septum, nucleus accumbens (NAcc), and VTA, among others (Bittencourt et al., 1992). LHA MCH neurons make connections to the insular cortex, nucleus of the solitary tract, parabrachial nucleus, and medial prefrontal cortex (Bittencourt et al., 1992). Connections to these regions involved in taste, olfaction and visceral sensation may contribute to the ability of MCH to regulate feeding (Shimada et al., 1998).

MCH acts in rodents through its only receptor, MCH receptor 1 (MCHR1; Bächner et al., 1999; Saito et al., 1999; Tan et al., 2002). MCHR1 is the only functional receptor for MCH in rats and mice, though MCHR2 is present in other mammals such as humans,

monkeys, dogs, and ferrets (Tan et al., 2002). MCHR1 is a G-protein coupled receptor (GPCR; Saito et al., 1999) and primarily acts postsynaptically by inhibiting adenylyl cyclase, phosphorylating extracellular signal-regulated kinases (ERKs), and promoting calcium mobilization to hyperpolarize cells via $G_{i/o}$ (Chambers et al., 1999; Hawes et al., 2000; Lembo et al., 1999; Saito et al., 1999) or G_q activation (Pissios et al., 2003). The distribution pattern of MCH-ir fibers is consistent with the expression pattern of the *Mchr1* mRNA (Kokkotou et al., 2001; Saito et al., 2001), as *Mchr1* is widely distributed throughout the brain with dense expression observed in the NAcc, hippocampal formation, basolateral amygdala, mammillary bodies, and locus coeruleus, among others (Saito et al., 2001). Moderate *Mchr1* expression is also observed in the ventromedial nucleus and arcuate nucleus of the hypothalamus (Arc) as well as the VTA (Saito et al., 2001). More recent analyses of *Mchr1* expression have shown that it is expressed on first-order neurons that regulate energy balance (Chee et al., 2013). For example, *Mchr1* expression is high in leptin-sensitive neurons of the Arc including first order primary neurons important for the regulation of energy balance such as neurons expressing proopiomelanocortin (POMC) and Neuropeptide Y (NPY; Chee et al., 2013). POMC neurons show greater colocalization with *Mchr1* expression than NPY neurons (Chee et al., 2013). In combination with the findings that MCH neurons of the LHA and innervated by NPY and POMC neurons of the Arc (Elias et al., 1998, 1999), this suggests these groups of neurons could form a reciprocal circuit that could form the basis of a feedback loop to modulate neuronal activity (Chee et al., 2013).

Interestingly, MCHR1 does not always need to be in the immediate vicinity of MCH neurons or MCH-ir fibers, as MCH may act via volume transmission, with MCH neurons releasing the MCH peptide into the ventricular system where it can travel to different brain regions (Noble et al., 2018). This presents an interesting characteristic of MCH neurons in that they show both classical synaptic signalling, via glutamate release, and volumetric signalling, via MCH release (Schneeberger et al., 2018).

1.1.2 Localization of MCHR1 protein expression on primary cilia

Recently, the emergence of a commercially available MCHR1 antibody allowed us to examine the distribution of MCHR1 protein. Overall, the pattern of MCHR1 protein is consistent with that for *Mchr1* mRNA with expression observed in the NAcc, hippocampal formation, and amygdala (Diniz et al., 2020). Interestingly, within these regions, MCHR1 is found on the cilia of neurons (Berbari et al., 2008; Diniz et al., 2020; Jasso et al., 2021; Kobayashi et al., 2021). Cilia are suggested to play a role in maintaining homeostasis by detecting and transducing stimuli (Berbari et al., 2009; Wheatley, 2008), and MCHR1 has been implicated as an important GPCR involved in cilia signalling but it has not yet been established to what end (Jasso et al., 2021). It has been shown that application of MCH can consistently initiate shortening of cilia (Kobayashi et al., 2021) while blocking or deleting MCHR1 has led to increased cilia length (Alhassen et al., 2021). Interestingly, optogenetic activation of MCH neurons has also shown to shorten cilia in cells with MCHR1 (Alhassen et al., 2021). Similarly, the increase of MCH mRNA within the LHA in fasting mice is correlated with cilia shortening in cells expressing MCHR1 (Kobayashi et al., 2021). It is possible cilia play a role in

regulating the activity of MCHR1 and fine-tuning the degree to which MCHR1 activation impacts neuronal activation.

1.2 Role of MCH in energy balance

1.2.1 MCH promotes food intake

Transgenic models of *Mch* overexpression or deletion are consistent with the orexigenic actions of MCH. Mice that overexpress *Mch* are more likely to overeat and become obese (Ludwig et al., 2001). In accordance with this, obese *ob*/*ob* leptin deficient mice also show increased *Mch* gene expression in the LHA (Qu et al., 1996). The obese phenotype of *ob*/*ob* mice can be attenuated by genetic deletion of *Mch* (Segal-Lieberman et al., 2003). Additionally, showing the opposite of mice with high *Mch* expression, *Mch* knockout mice (*Mch-KO*) show decreased food intake and are lean and hyperactive with an increased metabolic rate (Kokkotou et al., 2005; Shimada et al., 1998).

1.2.2 *Mchr1* deletion increases energy expenditure

Mchr1 knockout mice (*Mchr1-KO*) do not show the orexigenic effect of MCH application (Marsh et al., 2002). Knocking out *Mchr1* also results in lean hyperactive mice with increased energy expenditure, demonstrating MCHR1 is essential for MCH action (Chen et al., 2002; Marsh et al., 2002). Additionally, application of MCHR1 antagonists have shown to produce decreased weight and prevent diet-induced obesity in mice (Gomori et al., 2007; Ito et al., 2010; Mashiko et al., 2005). Interestingly, MCHR1 antagonist application has also been observed to decrease sucrose preference,

implicating MCH in nutrient sensing and reward associated with feeding (Karlsson et al., 2012).

1.3 Functional convergence of MCH and dopamine systems

1.3.1 Hyperdopaminergic state mediates hyperactivity following *Mch* or *Mchr1* deletion

Both *Mch* or *Mchr1* deletion consistently produced mice that are lean, hyperactive, and have increased energy expenditure. These effects are mediated by a hyperdopaminergic state. There is an elevated amount of dopamine (DA) in the NAcc of *Mch-KO* mice (Pissios et al., 2008) and *Mch-KO* rats (Mul et al., 2011). Furthermore, treatment with a DA reuptake inhibitor leads to a greater accumulation of DA at the NAcc following *Mch* deletion, and this can enhance and prolong hyperlocomotor activity (Pissios et al., 2008). These findings are consistent with recent evidence showing that MCH treatment can suppress DA release in the NAcc (Chee et al., 2019). Interestingly, MCH inhibition of DA release is no longer observed when *Mchr1* is deleted from GABAergic cells (Chee et al., 2019), thus suggesting that MCH can act via a GABAergic neurocircuit to inhibit DA release and deletion of *Mchr1* could disinhibit DA neurons to increase DA release (Chee et al., 2019). These results work hand-in-hand to demonstrate that disrupted MCH signalling is driven by a hyperdopaminergic state in the NAcc, and this is central to MCH-mediated energy expenditure.

1.3.2 Dopamine release by MCH neuronal activation is associated with sucrose preference

In addition to the regulation of energy balance, MCH neurons can also act on dopaminergic neurons for nutrient-sensing and food reward (Domingos et al., 2013). MCH neurons are sensitive to glucose as their activity increases with glucose levels (Burdakov et al., 2005; Kong et al., 2010). By examining animal preference for sucrose or sucralose, we can compare animal preference for a sweet drink with nutrient value to a similarly sweet tasting drink void of nutrients, respectively. Optogenetic activation of MCH neurons increases DA release at the NAcc and drives preference for sucrose over sucralose, demonstrating MCH neurons contribute to food reward by regulating DA neurons (Domingos et al., 2013). To confirm these findings were independent of taste, sweet-blind mice were tested, and activation of MCH neurons in these mice also showed a preference for the sucrose over sucralose (Domingos et al., 2013). Additionally, ablation of MCH neurons eliminates the increase in DA associated with sucrose consumption, further demonstrating MCH neurons modulate DA activity important for nutrient sensing and food reward (Domingos et al., 2013). Interestingly, *Mch-KO* mice do not show an altered sucrose preference and still prefer sucrose to sucralose (Schneeberger et al., 2018). Rather, glutamate release from MCH neurons is responsible for the reward associated with the nutrient value of sucrose (Schneeberger et al., 2018). These results highlight the importance of glutamatergic signaling from MCH neurons, thus MCH neurons may regulate dopaminergic activity via glutamate release.

1.3.3 MCH action throughout the mesocorticolimbic system

The mesocorticolimbic DA system is comprised of dopaminergic cells of the VTA projecting up through the medial-forebrain bundle to the NAcc and other cortical targets implicated in regulation of reward and motivation (Albanese & Minciacchi, 1983). Application of MCH onto the NAcc increases food intake and this effect is blocked when an MCHR1 antagonist is applied to inhibit MCH signalling (Georgescu et al., 2005). NAcc DA inputs originate in the VTA (Albanese & Minciacchi, 1983). Interestingly, ablation of MCH neurons in sweet-blind mice has also been shown to decreases the cFos expression, a marker of neuronal activity, in the DA neurons of the VTA associated with sucrose reward (Domingos et al., 2013). The findings discussed above implicate both the NAcc and VTA as potential targets of MCH action.

1.3.4 Neuroanatomical overlap of MCH and dopamine systems

There is neuroanatomical evidence that supports the convergence of MCH and DA systems. The NAcc shows both high *Mchr1* expression and MCH-ir fibers (Bittencourt et al., 1992; Hervieu et al., 2000; Saito et al., 2001). Similarly, moderate *Mchr1* mRNA expression and MCH-ir are both seen in the VTA (Hervieu et al., 2000). These neuroanatomical results support the potential for MCH and DA systems to converge and overlap as MCH fibers and *Mchr1* expression are both observed in major nodes of the mesocorticolimbic DA system. These findings suggest MCH machinery is present in both the NAcc and VTA, but these results are from experiments done in rats, and it would be important to assess the expression of *Mchr1* expression in the VTA of mice. Taken together, there is strong functional and anatomical evidence to support the

hypothesis that MCH can regulate DA neurons, and that one potential site of regulation is the VTA.

1.4 Cellular composition and regulation of VTA neurons

1.4.1 Cellular heterogeneity in the VTA

The VTA is roughly described as the area containing the A10 DA group (Dahlstroem & Fuxe, 1964). DA neurons projecting to the NAcc originate in the VTA (Albanese & Minciacchi, 1983). Despite being commonly thought of as exclusively dopaminergic, the VTA is a heterogeneous area comprised of dopaminergic, GABAergic, and glutamatergic neurons (Morales & Margolis, 2017).

VTA DA neurons are identified by the presence of tyrosine hydroxylase (TH), an enzyme required for the production of DA and expressed in high levels in VTA DA neurons (Margolis et al., 2006; Morales & Margolis, 2017). VTA neurons also express DA transporter (DAT) for DA reuptake and use the vesicular monoamine transporter 2 (VMAT2) to package DA into vesicles (Morales & Margolis, 2017). GABA neurons of the VTA typically express *Vgat* and utilize the protein to package GABA into vesicles, making *Vgat* a good marker of GABAergic cells (Morales & Margolis, 2017). It is also worth noting that GABA can utilize VMAT2 for packaging into vesicles (Tritsch et al., 2012). Similarly, glutamatergic VTA cells are typically identified by expression of *Vglut2* (Yamaguchi et al., 2007). Within the VTA, a population of neurons that can release both GABA and glutamate has also been identified (Root, Mejias-Aponte, Qi, et al., 2014; Yamaguchi et al., 2007). Interestingly, these GABAergic and glutamatergic neurons

seem more similar to VTA glutamate cells as they have a lower excitability and firing rate than GABA neurons of the VTA and require stronger excitation to fire than is required for GABA cells (Miranda-Barrientos et al., 2021). Additional subsets of VTA neurons that corelease DA and GABA (Stamatakis et al., 2013; Tritsch et al., 2012) and DA and glutamate (Dal Bo et al., 2004; Stuber et al., 2010; Sulzer et al., 1998; Tecuapetla et al., 2010) have also been found. Although heterogeneous, the VTA is not comprised into subnuclei based on the target of VTA projections (Albanese & Minciacchi, 1983) but rather, can be better described based on spatial organization of neuron types within the VTA based on medial-lateral, dorsal-ventral, and anterior-posterior differences (Morales & Margolis, 2017).

1.4.2 Regulation of VTA neurons by external and local projections

VTA neurons are regulated by both local circuitry and inputs from other regions. DA neurons of the VTA receive inputs from other regions and from local GABA and glutamate cells of the VTA (Morales & Margolis, 2017). VTA GABA neurons have been shown to inhibit DA neurons depending on expectation of reward (Cohen et al., 2012; Eshel et al., 2015; Tian et al., 2016) with decreased DA release at the NAcc as a result of activation of GABAergic VTA neurons (Van Zessen et al., 2012). Supporting this, inhibition of VTA GABA cells increases reward response in DA cells (Eshel et al., 2015). LHA projections to the VTA may also modulate DA neurons an ultimately influence motivation (Nieh et al., 2016). Lesioning the LHA mirrors DA depletion as both result in aphagia (Grossman et al., 1978; Stricker et al., 1978). Glutamatergic LHA projections may innervate VTA DA neurons (Kempadoo et al., 2013; You et al., 2001) as glutamate

receptor antagonists (NMDA blockers) in the VTA decreasing reward seeking behaviour (Kempadoo et al., 2013). However, mice will self-stimulate to activate GABAergic LHA projections to the VTA but not glutamatergic projections (Nieh et al., 2016). Interestingly, although glutamatergic and GABAergic neurons project to DA neurons, more are GABAergic than glutamatergic (Tepper & Lee, 2007). In line with this, increased inhibitory tone onto the VTA shows an increase in DA in the NAcc primarily driven by GABAergic LHA projections onto VTA GABA cells disinhibiting DA neurons (Nieh et al., 2016). Similarly, excitation of VTA GABA cells can be driven by glutamatergic LHA neurons (Miranda-Barrientos et al., 2021; Nieh et al., 2015). Interestingly, VTA glutamatergic neurons also receive glutamatergic inputs from the LHA (Barbano et al., 2020).

1.4.3 MCH action at the VTA

As MCH neurons are glutamatergic, a portion of glutamatergic LHA projections could represent MCH projections. MCH-ir is observed in the VTA (Bittencourt et al., 1992; Hervieu et al., 2000) and MCH afferents to the VTA have been identified (Faget et al., 2016). MCH projections to the VTA preferentially targeted non-GABA VTA cells and tended to innervate glutamate and DA VTA neurons (Faget et al., 2016). Moderate expression of *Mchr1* mRNA has also been observed in the VTA (Hervieu et al., 2000), thus implicating that MCH and DA circuits may overlap at the VTA. Indeed, MCHR1 has been detected at dopaminergic VTA cells (Diniz et al., 2020), but it is not known if *Mchr1* is preferentially expressed in specific cell types within the VTA. Extracellular recordings from rat VTA neurons did not reveal MCH action on the firing rate (Korotkova

et al., 2003), however, it is not clear if this is true in the mouse or with whole-cell recordings from TH-positive VTA neurons. Furthermore, MCH may impact other electrophysiological properties of VTA neurons and alter its excitability or synaptic inputs.

2. Rationale and Objectives

MCH has been shown to inhibit dopamine release within the striatum. However, it is not known if MCH can directly regulate the activity of dopaminergic neurons. We hypothesize that MCH can act directly on cells of the VTA and that the action of MCH will predominantly be at dopaminergic neurons as opposed to GABAergic and glutamatergic VTA cells. We will use a combination of molecular, neuroanatomical visualization, and electrophysiological techniques to assess MCH action in the VTA via the following specific aims:

Aim 1. To determine the expression and distribution of *Mchr1* in the VTA

To determine the neuroanatomical basis for MCH receptor expression in the VTA we will:

A. **Assess relative *Mchr1* mRNA expression in the VTA by quantitative RT-PCR**

   We will perform quantitative RT-PCR on tissue punches from the striatum, hypothalamus, cerebellum, and VTA to compare *Mchr1* gene expression in the gross anatomy of the VTA to regions known to show high, moderate, and low *Mchr1* expression, respectively. We will then confirm the presence of MCHR1 protein in these regions using immunohistochemistry.

B. Determine the expression of *Mchr1* on dopaminergic, GABAergic, and glutamatergic VTA cells by dual *in situ* hybridization and immunohistochemistry

We will perform *in situ* hybridization for *Mchr1* mRNA in combination with *in situ* hybridization for *Slc32a1* and *Slc17a6* and immunohistochemistry for TH to determine *Mchr1* expression on GABAergic, glutamatergic, and dopaminergic cells of the VTA, respectively. Expression will be mapped to the Allen Reference Atlas (Dong, 2008) and described in the anterior-posterior, medial-lateral, and dorsal-ventral axes.

Aim 2. To determine if MCH cells project to the VTA

We will inject a Cre-dependent retrograde adeno-associated virus (AAV) expressing mCherry into the VTA of *Mch-cr*e mice to label VTA-projecting MCH neurons. Furthermore, we will also determine if nerve terminals within the VTA that are labeled by synaptophysin may express MCH immunoreactivity.

Aim 3. To determine if MCH can inhibit dopaminergic, glutamatergic, or GABAergic VTA cells

We will perform whole-cell patch-clamp recordings in *Th-cre:L10-Egfp*, *Vgat-cre:L10Egfp*, and *Vglut2-cre:L10-Egfp* reporter mice and determine if MCH inhibits or suppresses synaptic input to dopaminergic, GABAergic, and glutamatergic VTA cells, respectively.

3. Methods

3.1 Animals

All animal procedures were approved by Carleton University's Animal Care Committee. All mice were group housed in a 12:12 hour light:dark cycle and ad libitum access to water and standard mouse chow (Teklad Global Diets 2014, Envigo, Mississauga, Canada) and water. Tissue for qPCR was collected from male (n = 6) and female (n = 6) wildtype (WT) mice 12–20 weeks old. Male WT mice 12–20 weeks old were used for MCHR1 immunohistochemistry (IHC; n = 3) and *Mchr1 in situ* hybridization (ISH) experiments (n = 3). *Mch-cre* mice (n = 3) 12–20 weeks old were injected to examine MCH projection to the VTA. Electrophysiological recordings were recorded from Male and female 4–10 week-old *Th-cre;L10-Egfp*, *Vgat-cre ;L10-Egfp*, and *Vglut2-cre;L10-Egfp* reporter mice. These mice were generated by crossing either heterozygous *Th-cre* (Jackson Laboratories, Bay Harbor, ME; JAX ID: 008601), *Vgat-cre* (Jackson Laboratories; JAX ID: 028862), or *Vglut2-cre* (Jackson Laboratories; JAX ID: 028863) mice to homozygotic Cre-dependent *lox-STOP-lox-L10-Egfp* reporter mice (Krashes et al., 2014), kindly provided by Dr. B. B. Lowell (Beth Israel Deaconess Medical Center, Boston, MA). The mice from this cross uniquely express the *Egfp:L10* gene in *Th*, *Vgat*, or *Vglut2* neurons, respectively.

3.2 Quantitative RT-PCR

3.2.1 RNA extraction

WT mice were anesthetized with an intraperitoneal injection of 7% chloral hydrate (700 mg/kg) prepared in sterile saline (0.9% NaCl) and the brain was dissected. Microdissected samples from the striatum, hypothalamus, cerebellum, and VTA were collected and flash-frozen in liquid nitrogen. Tissue samples were homogenized in 1 ml of TRIzol (#15596018, Invitrogen, Carlsbad, CA, USA) 200 ul of chloroform was then added to all the RNA, DNA, and protein to separate into different layers. Samples were centrifuged for 15 min at 4 °C at 10000 rpm and the upper aqueous layer containing RNA was removed. 500 µl of isopropanol was added to precipitate RNA and samples were centrifuged again for 15 min. Supernatant liquid was removed and RNA was washed with 1 ml of 70% EtOH. Samples were centrifuged again for 5 min and the supernatant was removed. Pellets were allowed to dry for approximately 10 min and resuspended in 50 µl of distilled (DI) water.

3.2.2 cDNA synthesis

To assess purity of RNA, a NanoDrop Lite Spectrophotometer (#ND-LITE-PR, Thermo Scientific, Waltham, MA) was used to confirm a reading of approximately 2 for the the 260/280 ratio. RNA concentration was also measured and aliquots of each sample were prepared with a concentration of 17.86 ng/µl. An additional sample of the RNA with the highest concentration was prepared to serve as a no-RT control. Samples were treated with 2 µl of iScript DNase prepared in DNase buffer (iScript gDNA Clear cDNA Synthesis Kit; #1725035, Bio-Rad, Hercules, CA). Samples were centrifuged and then

incubated in a thermal cycler with a heated lid. The incubation protocol consisted of a 5 min DNA digestion step at 25 °C, a 5 min DNase inactivation step at 75 °C, and then temporarily held at 4 °C prior to cDNA synthesis.

3.2.3 Quantifying *Mchr1* expression

A 4 µl volume of iScript Reverse Transcription Supermix (iScript gDNA Clear cDNA Synthesis Kit; #1725035, Bio-Rad) was added to each 16 µl RNA sample except the no-RT control which received 4 µl of iScript No-RT Control Supermix (iScript gDNA Clear cDNA Synthesis Kit; #1725035, Bio-Rad). Samples were centrifuged and incubated in a thermal cycler for 5 min at 25 °C, 30 min at 42 °C, 5 min at 85 °C, and temporarily held at 4 °C. cDNA was stored at –80 °C until used.

We performed quantitative RT-PCR using Sso Advanced Universal SYBR Green Supermix (#1725271, Bio-Rad). Primers for glyceraldehyde-3-phosphate dehydrogenase (*Gapdh*) and *Mchr1* were obtained from Invitrogen using the following sequences:

	Forward	Reverse
Gapdh	ATGTGTCCGTCGTGGATCTGA	ATGCCTGCTTCACCACCTTCTT
Mchr1	CAATGCCAGCAACATCTCC	ACCAAACACTGAAGGCATGA

A 10 µM primer mix was made by combining 10 µl of forward and reverse primer with 80 µl of RNase free water. A master mix of 0.4 µl of primer mix, 5 µl of SYBR Green Supermix, and 3.6 µl of water was made for each sample and 9 µl was added to 1 µl of

cDNA. Samples were incubated in a CFX Connect Real-Time PCR Detection System (#1855201, Bio-Rad) thermal cycler using the following protocol:

Step	Temperature (°C)	Duration (sec)
1	95	60
2	95	5
3	60	20
4	Go back to step 2, 39 cycles	
5	65	5
6	95	50
7	4	∞

Relative mRNA expression was calculated via double delta Ct analysis and normalized to expression levels of the housekeeping gene *Gapdh*.

3.3 Stereotaxic injections

Mch-cre mice (12–20 weeks old, n = 3) were anesthetized with isofluorane, given a subcutaneous injection of slow-release meloxicam (4 mg/kg; Metacam, Boehringer Ingelheim, Ingelheim am Rhein, Germany), every 72 hr as needed, and placed in a mouse stereotaxic frame. We unilaterally injected a retrograde AAV (50 nl; 25 nl/min; n = 2) encoding Cre recombinase-mCherry (AAVrg-flox-hChR2(H134R)-mCherry-WPRE-HGHpA; 20297, Addgene, Watertown, MA) into the rostral (in mm: anteroposterior (AP) –2.9, mediolateral (ML) –0.70, dorsoventral (DV) –4.6) and caudal VTA (AP –3.3, ML –0.4, DV –4.6) using mouse atlas coordinates (Paxinos 2014). Similarly, we unilaterally injected an AAV (200 nl; 50 nl/min; n = 1) encoding Cre-recombinase-synaptophysin-EYFP (AAV8-EF1a-DIO-synaptophysin-EYFP; UNC Gene Therapy Center Vector Core, Chapel Hill, NC) into the LHA (in mm: AP –1.1, ML –0.6, DV –5.2) using mouse atlas

coordinates (Paxinos 2014). Mice were single-housed and the virus was allowed to incubate 6 weeks before mice were sacrificed by transcardiac perfusion for histological analysis.

3.4 Tissue preparation for immunolabeling and *in situ* hybridization

Mice were anaesthetized with an intraperitoneal injection of 7% chloral hydrate (700 mg/kg) prepared in sterile saline (0.9% NaCl) and perfused with cold (4 °C) sterile saline (0.9% NaCl;) followed by cold (4 °C) phosphate buffered formalin (10%; VWR, Radnor, PA). WT brains for MCHR1 protein IHC were removed and post-fixed in a 20% sucrose formalin solution for 4 hr. Brains were then transferred to phosphate buffered saline (PBS, pH 7.4) with 20% sucrose until slicing. Injected brains and WT brains for ISH were extracted and post-fixed in 10% formalin overnight before being transferred to a phosphate buffered saline containing 20% sucrose solution and 0.5% sodium-azide for 24 hr for cryoprotection.

The brains were then sliced using a freezing microtome (Spencer Lens Co., Buffalo, NY) into five series of 30 µm coronal sections. Brains for IHC were stored in a 30% sucrose antifreeze solution at –20 °C until use. Sections designated for ISH were immediately mounted onto Superfrost Plus microscope slides (Superfrost Plus, Fisher Scientific, Pittsburgh, PA), air-dried for one hour at room temperature (RT; 21–23 °C) and then at –20 °C for 30 min before being stored at –80 °C until needed. ISH brain tissue series were kept in order and used for Nissl staining, RNAscope probe tissue,

and RNAscope negative control tissue, respectively. All brains had one series reserved for Nissl staining for neuroanatomical analysis.

3.5 Immunohistochemistry

WT tissue was stained for MCHR1 and counterstained with a fluorescent nissl (Neurotrace). *Mch-cre* tissue collected following injection of a retrograde AAV were stained for mCherry (labelled by Alexa fluor 488) and MCH (labelled by Alexa Fluor 594), and counterstained for DAPI. *Mch-cre* tissue collected following injection of a synaptophysin-EYFP AAV were stained for YFP (labelled by Alexa fluor 488) and MCH (labelled by Alexa Fluor 647).

IHC was performed based on protocol used by (Diniz et al., 2020). Slices were rinsed in PBS for 5 min, six times, incubated in a 0.3% solution of hydrogen peroxide in PBS for 20 min, and rinsed in PBS for 10 min, three times. Slices were then incubated at 4 ºC for 48 hr with an rabbit anti-MCHR1 (1:1000; PA5-24182, Invitrogen, Carlsbad, CA), chicken anti-mCherry (1:2000; #632496, Lot 1805080, Clontech, Mountain View, CA), or chicken anti-GFP (1:2000; #06-896, Lot 3022861, Millipore, Burlington, MA) primary antibody in a 3% normal donkey serum (NDS; #AB_2337258, Jackson ImmunoResearch, West Grove, PA) PBS-azide solution with 0.3% Triton to label MCHR1, mCherry, or YFP, respectively. Tissue was rinsed for 5 min in PBS, six times, and incubated for 1 hr at RT with biotinylated donkey anti-rabbit IgG antibody (1:500; #711-065-152, Lot 101909, Jackson ImmunoResearch) or biotinylated donkey anti-chicken antibody (1:500; #703-065-155, Lot 134054, Jackson ImmunoResearch) in a

3% NDS PBS solution with 0.3% Triton (PBT). Slices were rinsed in PBS for 10 min, three times, and incubated at RT for 30 min in an avidin-biotin-horseradish peroxidase solution (1:1:833; Vectastain Elite #PK-6100, Vector, Burlingame, CA). Slices were then washed three times for 10 min each and incubated at RT for 20 min in a 0.5% biotinylated (EZ-Link sulfo-NHS-LC-biotin; ThermoFisher Scientific, Waltham, MA) tyramine (Sigma-Aldrich; Sigma Chemical; St. Louis, MO, USA) hydrogen peroxide (0.005%) solution prepared in PBT. Sections were then incubated at RT for 2 hr with Alexa Fluor 647-conjugated streptavidin (1:500; #016-600-084, Lot 135095, Jackson ImmunoResearch) and neurotrace (1:50; #N21479, Fisher Scientific), or Alexa Fluor 488-conjugated streptavidin (1:500; #S32354, Lot 51924A, Invitrogen) prepared in PBT, and washed in PBS for 10 min, three times. The WT tissue stained for MCHR1 was then mounted onto Superfrost Plus microscope slides and cover-slipped with Prolong Diamond Antifade mounting media (#P36961, Invitrogen). Injected *Mch-cre* tissue was incubated in an anti-rabbit MCH primary antibody (1:2000; kindly provided by Dr. E. Maratos-Flier, Beth Israel Deaconess Medical 155 Center; RRID: AB_2314774; Chee et al., 2013; Elias et al., 1998) in 3% NDS in PBT-azide for 24 hr at RT. Slices were washed in PBS for 5 min, six times, and incubated for 2 hr at RT in a donkey anti-rabbit Alexa Fluor 594 (1:500; # A21207, Lot 567295, Invitrogen) or donkey anti-rabbit Alexa Fluor 647 (1:500; # A31573, Lot 1903516, Invitrogen) secondary prepared in 3% NDS PBT solution. Sections were washed in PBS three times for 10 min and then mounted and cover-slipped with Prolong Diamond Antifade mounting media with Dapi (#P36962, Invitrogen) or Prolong Diamond Antifade mounting media lacking DAPI.

3.6 Dual *in-situ* hybridization and immunohistochemistry

To examine the distribution and overlap of *Mchr1, Vgat, Vglut2*, and TH within the VTA, we utilised RNAscope to perform a triple *in situ* hybridization for *Mchr1*, *Slc32a1* (*Vgat*), and *Slc17a6* (*Vglut2*), mRNA with additional IHC for TH. Series 3 was designated as the Nissl with series 1 and 2 used as negative and experimental probe tissue, respectively. This was done so that the probe tissue would be adjacent (separated by only 30 µm) to both the negative control tissue and the parcellated Nissl tissue. One slide from an unused series was designated as a positive control. Procedures were based on manufacturer instructions for performing RNAscope *in situ* hybridization on fixed-frozen mouse brain tissue (Advanced Cell Diagnostic, 2019) and for adding IHC to this procedure (Advanced Cell Diagnostics, 2020).

3.6.1 Pretreatment and target retrieval

Tissue was removed from –80 °C storage and placed in a thermostat at 37 °C for 45 min to promote adhesion to the slide. Sections were then dehydrated in an ethanol gradient (50%, 70%, 100%; 5 min each). Slides were manually moved up and down in plastic coplin staining jars (Fisher Scientific) for all washes during this experiment to protect tissue quality. Following the ethanol, slides were allowed to dry for 5 min at RT and 5–8 drops of Hydrogen Peroxide (#323110, ACD) was added to cover each slide. Tissue was allowed to incubate at RT for 10 min and then washed twice in DI water for 5 min. We followed the target retrieval procedure in the RNAscope manual to promote better hybridization as our tissue was fixed-frozen. One coplin jar of DI water and another of 1x target retrieval (#32000, ACD) were heated in an Oster steamer (Jarden,

Rye, NY) set to 99 °C. The slides were initially placed in the heated DI water for 10 sec, to acclimate the tissue to the temperature change, and then transferred to the heated 1x target retrieval for 5 min. The slides were then transferred to DI water for 15 s to cool down prior to a 3 min dehydration in 100% ethanol. Slides were air dried at RT overnight.

3.6.2 Probe hybridization

The following morning, to keep reagents on the tissue, a hydrophobic barrier was drawn around the sections containing the VTA using an Immedge hydrophobic barrier PAP pen (Vector Laboratories, Burlington, CA) and allowed to dry for 10 min. A volume of 5–8 drops of Protease III (#322381, ACD) was added to each slide and incubated for 30 min in a HybEZ oven at 40 °C (#310010, ACD). Following incubation, slides were washed for 3 min in DI water, twice. Hybridization of *Mchr1*, *Vgat*, and *Vglut2* mRNA was performed using the *Mm-Mchr1-C1* (#317491, ACD), *Mm-Slc32a1-C2* (#319191-C2, ACD), and *Mm-Slc17a6* (#319171-C3, ACD) probes, respectively. The concentrated *Vgat* C2 and *Vglut2* C3 probes were both added in to the already diluted *Mchr1* probe at a ratio of 1:50. A volume of 5–8 drops of the probe mixture was added to each slide. Dihydrodipicolinate reductase (dapB, #313919, ACD) was used in place of the probes as the negative control on Series 1 tissue, and a probe for peptidyl-prolyl cis-trans isomerase B (PPIB) mRNA, *Mm-PPIB* (PPIB; #313919, ACD), was added to the positive control slide. The slides were then put in the HybEZ oven at 40 °C for 2 hr. After incubation, slides were washed three times in 1x wash buffer for 2 min each time.

3.6.3 Amplification

To amplify signal, 5–8 drops of AMP-1 (#323110, ACD) was added to each slide and they were put back in the 40 °C oven for 30 min. The slides were then washed twice in 1x wash buffer for 2 min each time. 5–9 drops of AMP-2 (#323110, ACD) were added to each slide and they were incubated in the 40 °C oven for 30 min. The slides were washed in wash buffer twice more for two minutes each time, then 5–8 drops of AMP-3 (#323110, ACD) were added to each slide and incubated at 40 °C for 15 min. Slides were washed two times, 2 min each time, in wash buffer.

3.6.4 Channel 1 signal development

To label *Mchr1* hybridization in channel 1, 5–8 drops of HRP-C1 (#323110, ACD) was added to all slides and incubated for 15 min in the oven (40 °C). Slides were washed twice, 2 min each time, in wash buffer. 200 µl of a 1:750 solution of tyramide signal amplification (TSA) plus Opal 690 (FP1497001KT, Akoya Biosciences, Marlborough, Massachusetts) in TSA buffer (#322809, ACD) was added to each slide and they were incubated for 30 min in the 40 °C oven. Slides were washed two times for 2 min in wash buffer and 5–8 drops of HRP Blocker (#323110, ACD) was added to each slide. Slides were then incubated in the oven at 40 °C for 15 min. Slides were washed two times, 2 min each time, in wash buffer.

3.6.5 Channel 2 signal development

To label *Vgat* hybridization in channel 2, 5–8 drops of HRP-C2 (#323110, ACD) was added to all slides and incubated for 15 min in the oven (40 °C). Slides were washed

twice, 2 min each time, in wash buffer. 200 µl of a 1:1500 solution of tyramide signal amplification (TSA) plus Cyanine 3 (NEL44E001KT, PerkinElmer, Waltham, Massachusetts) in TSA buffer was added to each slide and they were incubated for 30 min in the 40 °C oven. Slides were washed two times for 2 min in wash buffer and 5–8 drops of HRP Blocker was added to each slide. Slides were then incubated in the oven at 40 °C for 15 min. Slides were washed two times, 2 min each time, in wash buffer.

3.6.6 Channel 3 signal development

To label *Vglut2* hybridization in channel 3, 5–8 drops of HRP-C3 (#323110, ACD) was added to all slides and incubated for 15 min in the oven (40 °C). Slides were washed twice, 2 min each time, in wash buffer. 200 µl of a 1:750 solution of tyramide signal amplification (TSA) plus Opal 520 (FP1487001KT, Akoya Biosciences) in TSA buffer (#322809, ACD) was added to each slide and they were incubated for 30 min in the 40 °C oven. Slides were washed two times for 2 min in wash buffer and 5–8 drops of HRP Blocker was added to each slide. Slides were then incubated in the oven at 40 °C for 15 min. Slides were washed two times, 2 min each time, in wash buffer.

3.6.7 Immunohistochemistry for TH

Following *in situ* hybridization of the probe tissue, we performed an IHC stain for TH based on the procedure outlined by ACD for combining RNAscope with IHC (Document 323100-TN, ACD). A 3% NDS solution in PBS was prepared and 700 µl was pipetted onto each slide. Slides were allowed to incubate for 30 min at RT to block the tissue. The anti-sheep TH antibody (GTX82570, Lot 822005648, GeneTex, Irvine, California)

was then prepared in 3% NDS solution at a concentration of 1:1000. Blocking solution was removed from the slides and 700 µl of the prepared primary antibody was added. Tissue was left to incubate at room temperature for 2 hr and then washed, twice, in PBS for 2 min each time. We used an Alexa 594 anti-sheep (#715-496-150, Lot 82079, JacksonImmuno Research) as our secondary antibody, which we prepared at a 1:500 concentration in 3% NDS. A volume of 700 µl of the secondary solution was pipetted onto each slide and allowed to incubate at RT for 30 min. Slides were then washed for 2 min in wash buffer, twice. Approximately 4 drops of RNAscope DAPI Reagent (#323110, ACD) were added to the slides at RT for 30 sec and the slides were then immediately cover-slipped with ProLong Gold Antifade Mountant (Fisher Scientific). Slides were kept in a dark drying drawer at RT overnight and then stored at –20 °C.

3.7 Nissl stain

Sections underwent Nissl staining based on previously established procedures (Negishi et al., 2020). Slides were removed from storage at –80 °C and placed in an incubator (Fisher Scientific) at 37 °C for 45 min. The tissue was then dehydrated by treating the slides with an ethanol gradient of 50%, 70%, 95%, and three exchanges of 100% ethanol for 3 min each. Tissue was then delipidized in xylene (Millipore Sigma), first for 10 min and then for an additional 15 min in a fresh xylene exchange. Sections were then rehydrated down an ethanol gradient (100%, 95%, 70%, 50%, %; 3 min each) and into DI water for 3 min to rehydrate. The tissue was then dipped, for 30 s, in a 0.25% thionine solution (Kiernan, 2001), made from thionin acetate salt (Millipore Sigma). Slides were then washed in a bath of DI water to examine the stain. If too dark, slides

were dunked in 4% acetic acid. If staining was too light, it was dipped back in the thionin. The stain was adjusted until it took on a vivid violet colour with white matter distinguishable by eye. Sections were transferred to a DI water bath before being dehydrated in an EtOH gradient again (50%, 70%, 95%, 100%, 100%, 100%, %; 3 min each). Slides were then submerged in xylene for 10 min and another 15 min in a fresh bath of xylene before being cover-slipped using Mounting Medium (Richard-Allan Scientific, Fischer Scientific) and allowed to dry. Finished slides were labelled and stored at RT.

3.8 Imaging

All IHC and ISH images were acquired using a Nikon C2Si (Nikon, Tokyo, Japan) confocal affixed to a Nikon Eclipse Ti2-E microscope (Nikon) and processed using NIS-Elements Imaging Software (Nikon). Stitched large-image 10x brightfield photomicrographs of whole Nissl-stained sections were acquired using a DS-Ri2 color camera (Nikon) affixed to a Nikon Eclipse Ti2-E microscope and processed using NIS-Elements as well. 10x or 20x high resolution IHC and ISH images of specific regions were obtained as outlined below. Confocal 4x 405 nm stitched large-images of the entirety of each IHC and ISH section were also acquired to be aligned to adjacent Nissl images and transfer Nissl-based parcellations onto 10x or 20x high resolution images. All images were saved and exported as TIFF files.

3.8.1 Imaging MCHR1, mCherry, EYFP, and MCH IHC

The 10x and 20x large stitched images of regions of interest were acquired for both the MCHR1 stained tissue and injected tissue. MCHR1 labelled by Alexa Fluor 647 was imaged at 647 nm and fluorescent Nissl (Neurotrace) staining was imaged at 405 nm. Tissue injected with a retrograde AAV expressing mCherry underwent IHC staining for mCherry in combination with MCH to confirm viral expression is observed in neurons expressing MCH. mCherry labelled by Alexa Fluor 488 was imaged at 488 nm and pseudocoloured red, MCH labelled by Alexa Fluor 591 was imaged at 591 nm and pseudocoloured green, and DAPI was imaged at 405 nm. Images of MCH neurons in the LHA were captured. Tissue injected with AAV synaptophysin-EYFP was stained for MCH in combination with YFP to confirm synaptophysin expression in MCH fibers. YFP signal labelled by Alexa Fluor 488 was imaged at 488 nm and MCH labelled by Alexa Fluor 647 was imaged at 647 nm. Images of MCH fibers in the VTA were captured.

3.8.2 Imaging RNAscope tissue

The positive control was imaged to confirm hybridization and assess RNA quality. *Mchr1* mRNA hybridization labelled with Opal 690 was imaged at 647 nm, *Vglut2* hybridization labelled with Opal 520 was imaged at 488 nm, and the DAPI was imaged at 405 nm. *Vgat* hybridization labelled with Cy3 and the TH IHC labelled with Alexa Fluor 594 were both imaged with continuous band (CB) settings using an adjustable 591 nm laser so that they could be separated using spectral unmixing. CB acquisitions using 10 nm bins, from 570–630 nm were used to image Cy3 and Alexa Fluor 594 signal. CB acquisitions were then spectrally unmixed to separate these signals using

region-of-interest defined spectra for Cy3 and Alexa Fluor 594 from each section of tissue. CB acquisitions were obtained at the same time and using the same coordinates used to image the 405, 488, and 647 nm channels so the spectrally unmixed channels could be merged and aligned with these other channels into one file that displayed all five targets. The 20x stitched, large-image microphotographs of the VTA from each section of the probe series were also acquired this way.

The 20x sample images of the VTA from each section in the negative tissue were then acquired using this same imaging process. To subtract any background fluorescence caused by non-specific binding and ensure the validity of ISH signal, the 488, Cy3, and 647 channels of the negative images were adjusted until they did not show any background fluorescence and appeared black. The look up table values (LUTs) that resulted in a black image were recorded for each negative section and averaged for each of these channels. These negative LUT values were then applied the series 2 probe images. Images of all the sections containing the VTA, for both negative and probe series, were acquired using the same settings to ensure they can be compared and differences were not due to a difference in magnification, scan area, laser power, or gain.

3.9 Neuroanatomical analyses

3.9.1 Parcellations

Nissl images were parcellated (Figure 1) in Adobe Illustrator CS6 (Adobe Inc., San Jose, CA) using a digital drawing pad (WACOM, Kazo, Saitama, Japan). Based on the regions and subregions defined in the Allen Reference Atlas (ARA; Dong, 2008) but according to the unique cytoarchitectural features (including cell morphology, directionality, size, and intensity of staining) specific to the stained tissue, neuroanatomical boundaries were drawn.

3.9.2 Aligning and transferring parcellations to probe tissue

Probe images were imported into the corresponding Nissl Adobe Illustrator file so that the images of experimental IHC or ISH tissue could be aligned with its adjacent Nissl-stained tissue, at which point the parcellations could be transferred onto the probe images (Figure 1). As the high-resolution images of a portion of the slice cannot be properly aligned to the adjacent Nissls but can be easily aligned to the 4x whole section images, we first aligned the large 4x 405 nm images to the Nissl images (Figure 1). White matter, ventricles, blood vessels, and other easily identifiable landmarks were used to ensure slices were properly aligned. The high-resolution images could then be aligned to the 4x 405 nm images by aligning Dapi signal (Figure 1). For each section, all the channels for a high-resolution image were imported all at once and grouped to keep them aligned, allowing for different channels to be toggled on and off. Once the high-resolution image was aligned with the 4x and Nissl, the parcellations drawn from the

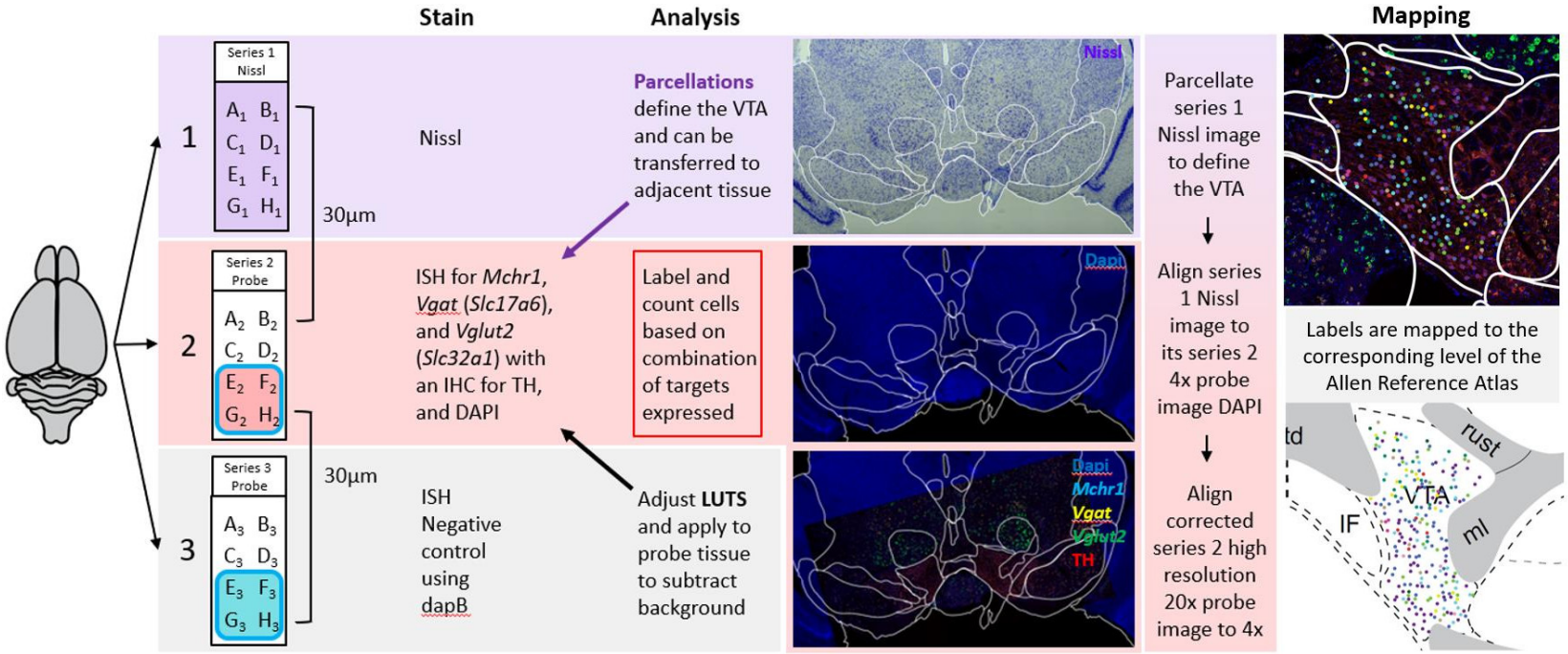

Figure 1. Schematic of neuroanatomical processing and analysis. Nissl-stained tissue was parcellated (Series 1) and aligned to an adjacent brain series that was hybridized and immunostained (Series 2). Fluorescence hybridization signals were subtracted from background fluorescence determined within a subsequent brain series that was hybridized to a negative control probe (Series 3).

Nissl series were transferred onto the experimental probe tissue to define the unique neuroanatomical boundaries of this tissue.

3.9.3 Identifying and labelling neurons

MCHR1 protein appeared as thick curved line fragments colocalized with cell bodies labelled by the fluorescent Nissl stain. One or more copies of MCHR1 colocalized to a cell body was considered an MCHR1 cell. We exclusively examined signal within the boundaries of the VTA. LHA neurons expressing mCherry were labelled as MCH+ by examining overlap of mCherry and MCH signal. mCherry and MCH both label whole cell bodies and colocalization with a Dapi-labelled nucleus was used to confirm signal was colocalized on a neuron. MCH fiber in the VTA appeared as long fibers of passage and punctate signal indicative of terminal boutons. Synaptophysin-EYFP expression appeared as dots colocalized to MCH fibers.

Analysing RNAscope tissue, we used the ellipse tool in Adobe Illustrator to label neurons within the VTA for every slice containing the VTA (Figure 1). We labelled neurons by examining one probe at a time and establishing criteria for each of the different targets. ISH signal criteria was established based on the prevalence of signal to background. *Mchr1* hybridization was imaged in the 647 nm channel and was pseudocoloured cyan to help with visualization. *Mchr1* signal appeared as punctate cyan dots with clusters centered tightly around Dapi-labelled nuclei. Clusters of 3 or more dots colocalized with a nucleus were labelled as neurons expressing *Mchr1* mRNA; *Mchr1* neurons were labelled with a blue elipse. Hybridized *Vgat* appeared as collections of punctate yellow dots and many formed collections in the shape of cell

bodies. Labelling the ISH for *Vgat* in the Cy3 channel, we looked for clusters of 5 or more dots that were colocalized to a Dapi-labelled nucleus. *Vgat* neurons were labelled yellow. Labelling the ISH for *Vglut2* in the 488nm channel, expression was observed more sporadically and often less concentrated around nuclei than the *Vgat* expression. We labelled collections of 4 dots or more that surrounded a Dapi-labelled nucleus as being *Vglut2* positive. *Vglut2* neurons were labelled green. Labelling the Alexa 594 channel with the IHC for TH, we labelled neurons based on the shape and intensity of staining, with signal in the shape of a cell body colocalized with a Dapi-labelled nucleus being deemed TH neurons. TH neurons were labelled red.

We then systematically assessed the overlap of these different targets and labelled neurons based on what combination they expressed. To help determine the colocalization of multiple targets, we adjusted the opacity of the images to be “screen” in Adobe Illustrator, allowing the images to be viewed on top of one another and examine if expression of multiple targets was observed on the same neuron. If we confirmed two labels were on the same neuron, the multiple labels were removed and replaced with one of a different colour indicating the combination of targets it expresses. We identified the following types of neurons expressing two targets; *Mchr1* and TH; *Mchr1* and *Vgat*; *Mchr1* and *Vgat*; TH and *Vgat*; TH and *Vglut2*; *Vgat* and *Vglut2*. We identified the following neurons expressing three targets: *Mchr1*, TH, and *Vgat*; *Mchr1*, TH, and *Vglut2*; *Mchr1*, *Vgat*, and *Vglut2*; TH, *Vgat*, and *Vglut2*. Finally, we labeled those cells that expressed all 4 markers (*Mchr1*, *Vgat*, *Vglut2*, TH). Each cell type was kept in its own separate sublayer so each population could be easily toggled on and off and counted.

3.9.4 Mapping

The identity and location of labelled neurons and fibers were transferred onto the corresponding level of the ARA to map the observed distributions on standardized atlas plates (Figure 1). All the labels were relegated to their own layer in the original working Illustrator file so that they could all be copied at once in a manner that conserved their relative position to each other. This label layer was copied into a new Illustrator file with the corresponding atlas plate. The collective of labels was then resized and adjusted, at first as a whole and then in smaller portions, to make the representation of the experimental VTA fit to the atlas VTA. This way, despite physical differences unique to the animal (such as size and shape of brain regions), neurons and fibers were mapped to their correct position relative to the neuroanatomical boundaries.

3.9.5 Quantification

The different cell types labelled were all counted for each atlas level. Cell counts are unilateral and based on mapped expression. Totals and percentages were calculated in Google Sheets (Google, Mountain View, California) and graphed using Prism 8 (GraphPad, San Diego, CA).

3.10 Electrophysiology

3.10.1 Acute brain slice preparation

Mice were anaesthetized with an intraperitoneal injection of 7% chloral hydrate (700 mg/kg) prepared in sterile saline (0.9% NaCl) and perfused with NMDG-HEPES slice solution (300 mOsm/L; containing (in mM): 92 NMDG, 2.5 KCl, 1.25 NaH_2PO_4, 30

$NaHCO_3$, 20 HEPES, 25 glucose, 2 thiourea, 5 Na-ascorbate, 3 Na-pyruvate, 0.5 $CaCl_2 \cdot 2H_2O$, and 10 $MgSO_4$ (Ting et al., 2018) that had been chilled to 4 °C and carbogenated (95% O_2, 5% CO_2). Brains were rapidly dissected, blocked and mounted to facilitate coronal slicing on a vibratome (Leica VT 1000S, Leica Biosystems, Wetzlar, Germany). Making sure the mounted brain tissue was kept submerged in the chilled and carbogenated NMDG slice solution during slicing, coronal slices containing VTA were cut 250 µm thick and immediately transferred to a 37 °C solution of carbogenated NMDG slice solution for 5 min. Slices were then transferred to a 37 °C solution of carbogenated bath-artificial cerebrospinal fluid (ACSF; 300 mOsm/L; containing (in mM) 124 NaCl, 3 KCl, 1.3 $MgSO_4$, 1.4 NaH_2PO_4, 10 D-glucose, 26 $NaHCO_3$, and 2.5 $CaCl_2$) for 5 min. Slices were then incubated at RT in carbogenated bath-ACSF for at least 1 hr prior to being used in patch-clamp experiments to promote recovery.

3.10.2 Patch-clamp recordings

Brain slices containing VTA were placed in a slice chamber that was superfused with carbogenated bath solution (2–2.5 ml/min, Master Flex CL Cole Palmer pump, Vernon Hills, IL) warmed to 37 ^oC by a temperature controller (Warner Instrument Corporation, Hamden, CT). Slices were held in place by a platinum ring strung with nylon fiber. Borosilicate glass pipettes (#593800; A-M Systems) were pulled on a P-1000 Flaming/Brown micropipette puller (Sutter Instruments; Novato, CA) and backfilled with a filtered potassium gluconate internal solution (290 mOsm/L, pH 7.24; containing (in mM) 120 K-gluconate, 10 KCl, 10 HEPES, 1 $MgCl_2$, 1 EGTA, 4 MgATP, 0.5 NaGTP, and 10 phosphocreatine) to assess membrane properties and glutamatergic events. A

cesium-based pipette solution (290 mOsm/L, pH 7.24; containing in mM) 128 CsMS, 11 KCl, 10 HEPES, 0.1 CaCl2, 1 EGTA, 4 MgATP, 0.5 NaGTP) was used to record GABAergic events. An Examiner.A1 microscope (Zeiss, Oberkochen, Germany) equipped with an AxioCam camera (Zeiss) and Axiovision software (Zeiss) was used to visualize cells using infrared differential interference contrast. Epifluorescence illumination (395–488nm) was used in combination with a 40x water immersion objective lens to identify and patch fluorescent EGFP neurons of the VTA (Figure 2A–C). Voltage- and current-clamp recordings of fluorescent neurons within the VTA were taken at –60 mV or –5 mV and recorded using a MultiClamp 700B amplifier (Molecular Devices, San Jose, CA) and digitized using a Digidata 1440A (Molecular Devices). Traces were acquired and filtered at 1 kHz by pClamp 10.3 software (Molecular Devices).

3.10.3 Drug application

Cells were constantly superfused with carbogenated bath-ACSF during a minimum 5 min baseline and allowed to stabilize prior to bath application of drug. A 3 μM MCH (H-1482, Bachem, Torrance, CA) solution was prepared using bath-ACSF and carbogenated prior to its 5–6 min application. An approximately 30 min washout in carbogenated bath-ACSF followed application of MCH to examine if its effects were reversible. In some current-clamp recordings, tetrodotoxin citrate (TTX; 500 nM; T-550; Alomone labs, Jerusalem, Israel) prepared in bath-ACSF was applied at least 10 min prior to MCH application and maintained over the entire recording. TTX was only added to cells that were hyperpolarized by a puff application of MCH.

3.10.4 Puff application

In experiments determining if MCH-mediated hyperpolarization is activity independent, we first delivered a short puff of 3 μM MCH to patched cells in order to identify MCH-sensitive cells. To deliver the MCH puff, a second pipette containing 3 μM MCH was positioned approximately 20–30 μm from the patched cell (Figure 2D) and gradual positive pressure was manually applied to the puff pipette for 5-10 seconds until the ripple of MCH was observed to reach the patched cell.

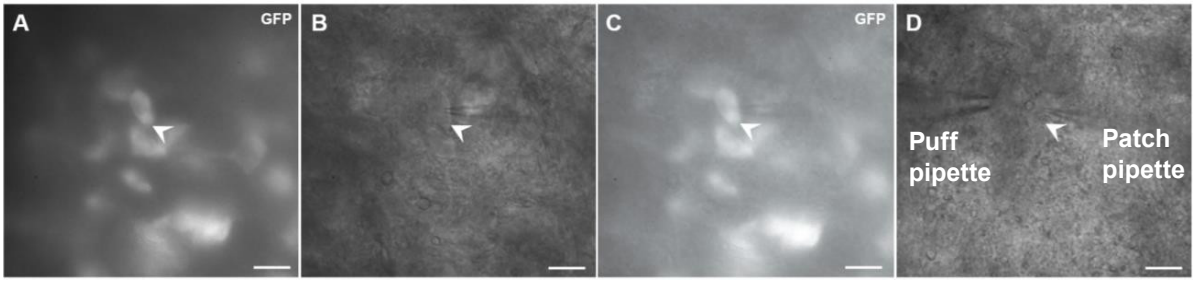

Figure 2. Recording from VTA neurons. Native eGFP fluorescence (**A**) in *Th-cre;L10-Egfp*, *Vgat-cre;L10-Egfp*, and *Vglut2-cre;L10-Egfp* reporter mice guided whole-cell patch-clamp recordings within the VTA (**B**). eGFP expression was confirmed in patched cells prior to recordings (**C).** A puff application of MCH applied via a second pipette positioned 20–30 μm next to patched cells aided in the detection of MCH-sensitive VTA (**D**). Scale bar: 20 μm.

3.10.5 Membrane potential analysis

Trace data was processed in Clampfit 10.7 (Molecular Devices) with membrane potential sampled every second and averaged into 15 s bins. Control value was the mean resting membrane potential (RMP) averaged over 5 min immediately prior to application of MCH. For puff experiments, membrane potential was sampled every 100 ms and averaged into 1 s bins. In puff experiments, control value was the mean RMP averaged over 5 s immediately prior to puff. Changes in resting membrane potential (Δ RMP) relative to baseline RMP values were analyzed and graphed using Excel 2016

(Microsoft) and Prism 9 (GraphPad). The Δ RMP observed with puff application was sampled 5–15 s after the puff. The Δ RMP observed in subsequent puffs (second MCH puff, ACSF puff, and MCH in TTX puff) were compared to the Δ RMP observed with the first MCH puff in the same cell using a paired *t* test.

3.10.6 Synaptic activity

Spontaneous excitatory postsynaptic current (sEPSC) events were recorded at –60 mV with a K-based internal, while inhibitory post synaptic currents (sIPSC) were recorded at –5 mV with a Cs-based internal. The frequency of EPSCs and IPSCs were analyzed using MiniAnalysis (Synaptosoft, Decatur, GA) and binned into 15 s increments. The control value was the mean event frequency averaged over 5 min immediately prior to application of MCH. Changes in frequency relative to baseline values were analyzed and graphed using Excel 2016 (Microsoft) and Prism 9 (GraphPad).

3.11 Graphs and figures

Graphs were prepared using Prism 9 (GraphPad), and figures were assembled in Adobe Illustrator 2020 (Adobe Inc.).

3.12 Statistics

Statistical significance was determined using Prism 9 (GraphPad). Group means were compared by unpaired or paired t-test where appropriate, and considered statistically significant at $p < 0.05$. All data are reported as group mean ± SEM.

4. Results

4.1 Expression and distribution of *Mchr1* in the VTA

4.1.1 Greater *Mchr1* mRNA expression in VTA of female mice

We quantified the expression of *Mchr1* in the hypothalamus, striatum, hippocampus, VTA, and cerebellum by RT-qPCR. *Mchr1* expression in each brain region was standardized to the expression of the housekeeping gene, *Gapdh*, and normalized to the level of *Mchr1* in the hypothalamus of the same mouse (Figure 3A). *Mchr1* expression in the striatum was over 3.5 fold higher than hypothalamic *Mchr1* expression (male: 3.6 ± 0.3, n = 5; p = < 0.0001; female: 4.4 ± 0.3, n = 6; p = < 0.0001) and barely detectable in the cerebellum (male: 0.0 ± 0.0, n = 6; female: 0.0 ± 0.0, n = 6). *Mchr1* expression in the VTA (male: 0.4 ± 0.1, n = 4; female: 0.6 ± 0.1, n = 6) was comparable to that in the hypothalamus (male: 1.0 ± 0.2, n = 6; p = 0.084; female: 1.0 ± 0.1, n = 6; p = >0.999) and hippocampus (male: 0.7 ± 0.1, n = 6; p = >0.999; female: 0.9 ± 0.0, n = 6; p = >0.999). Interestingly, *Mchr1* expression was nearly 2-fold higher in female (1.8 ± 0.3, n = 6) than male VTA (1.0 ± 0.1, n = 4; p = 0.044; Figure 3B).

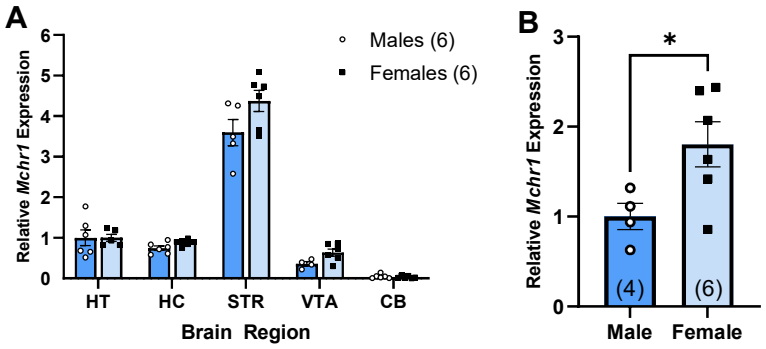

Figure 3. Higher *Mchr1* expression in the female VTA. *Mchr1* mRNA expression in the striatum (STR), hippocampus (HC), ventral tegmental area (VTA), and cerebellum (CB) of male and female wildtype mice was normalized to *Mchr1* expression in the hypothalamus (HT) (**A**). Direct comparison of *Mchr1* expression in the male and female VTA (**B**). Unpaired t test: *, p < 0.05.

4.1.2 MCHR1 protein is expressed in the VTA of male and female mice

We examined the expression of MCHR1 protein in the VTA of male (n = 1) and female (n = 1) WT mice by immunohistochemistry. There was robust MCHR1 expression in the VTA of WT male (Figure 4A) and female mice (Figure 4B). In addition to WT tissue, we performed IHC for MCHR1 on tissue from MCHR1-KO mice (male, n = 1; female, n = 1) to serve as negative controls. The absence of MCHR1 staining observed in MCHR1-KO tissue (Figure 4C) conferred the specificity of MCHR1 immunoreactivity in WT VTA tissue. Interestingly, MCHR1 immunoreactivity had a long and slender appearance and is consistent with MCHR1 expression observed on the primary cilia of neurons. These IHC stains confirmed the presence of MCHR1 protein in the VTA of male and female mice.

4.1.3 Neuronal composition of the VTA

We determined at least four major VTA cell types, including those that express TH, *Vgat*, *Vglut2*, or *Vgat*/*Vglut2*. *Vglut2* neurons are most abundant in the anterior VTA and are the most prevalent neuron type in the anterior VTA but quickly decrease in number and become the least prevalent in the middle and posterior VTA (Figure 5). TH and *Vgat* neurons are the most prevalent in the middle of the VTA and *Vgat* neurons have a relatively steady presence throughout the whole VTA but due to the smaller total cell count in the posterior levels, *Vgat* cells comprise the majority of VTA cells here (Figure 5). Overall, these three cell types are expressed in relatively similar numbers and proportions (Figure 5).

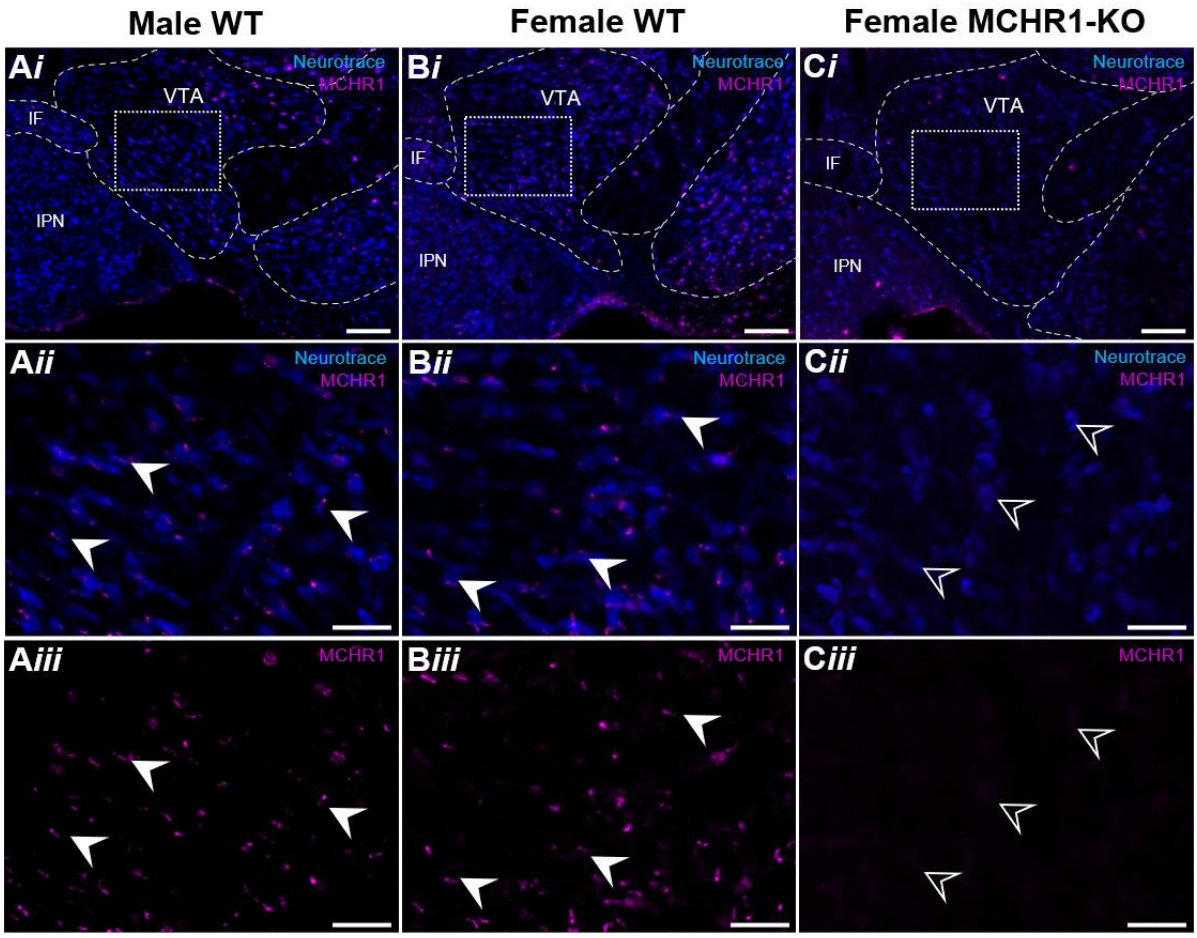

Figure 4. MCHR1 protein is expressed in the VTA. Confocal photomicrographs showing MCHR1 immunoreactivity and fluorescent Nissl (Neurotrace)-stained soma in the VTA of male WT (**A**), female WT (**B**), and female MCHR1-KO tissue (**C**) at low magnification (***i***) and high magnification image (***ii*** and ***iii***, from dotted, outlined region in ***i***). Representative examples of the presence (filled arrowhead) or absence (open arrowhead) of MCHR1 immunoreactivity at Neurotrace-labeled VTA soma (***ii***, ***iii***). Scale bars: ***i,*** 100 µm; ***ii*** and ***iii***, 40 µm. IF, interfascicular nucleus raphe; IPN interpeduncular nucleus; VTA, ventral tegmental area.

The three VTA cell types showed little overlap, with most neurons expressing exclusively TH*, Vgat*, or *Vglut2*. Although most combinations of TH, *Vgat*, and *Vglut2* were extremely uncommon, a constant presence of cells expressing both *Vgat* and *Vglut2* was observed and outnumber *Vglut2* cells in the posterior half of the VTA (L85–90; Figure 5). Interestingly, we also observed the presence of a small number of

TH/*Vglut2* neurons concentrated in this same region (L86–89; Figure 5). These TH/*Vglut2* neurons comprised only a small number of VTA cells counted (Figure 5) and were thus not further analyzed in detail here. A negligible number of neurons expressing TH and *Vgat* were also observed sporadically throughout the VTA.

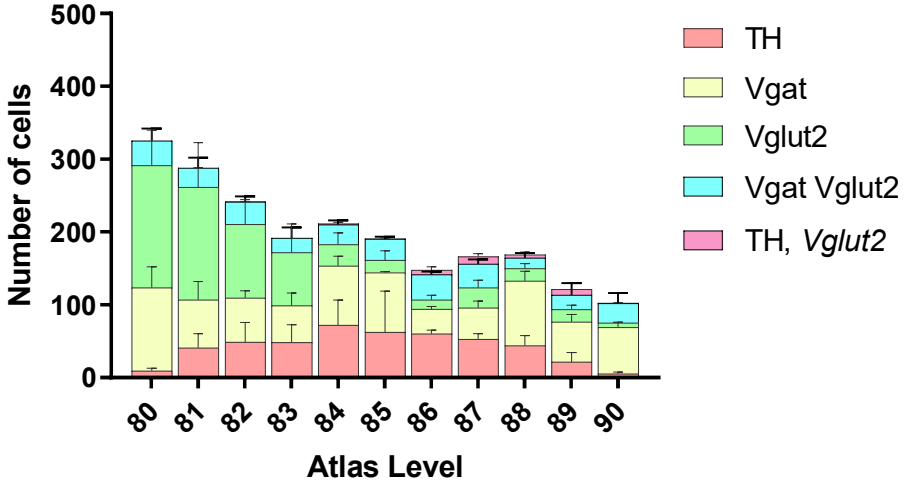

Figure 5. VTA composition and neurochemical characterization of the VTA *Mchr1* population. The number of cells throughout the VTA that express any combination of TH, *Vgat*, and *Vglut2*.

4.1.4 Expression of *Mchr1* mRNA in TH, *Vgat*, *Vglut2*, and *Vgat*/*Vglut2* VTA cells

We observed *Mchr1* expression in a variety of VTA cells types (Figure 6A, B*i*). We found that *Mchr1* hybridization signals (Figure 6B*ii*) colocalized with TH (Figure 6B*iii*, B*iv*), *Vgat* (Figure 6B*v*, B*vi*), and *Vglut2* (Figure 6B*vii*, B*viii*) cells (white arrowheads). We also observed *Mchr1* expression on VTA cells expressing both *Vgat* and *Vglut2* mRNA (Figure B*vi*, B*viii*; blue arrowhead). Interestingly, *Mchr1* hybridization also appeared in undefined VTA cells (Figure 6B*i* and 6B*ii;* open arrowhead).

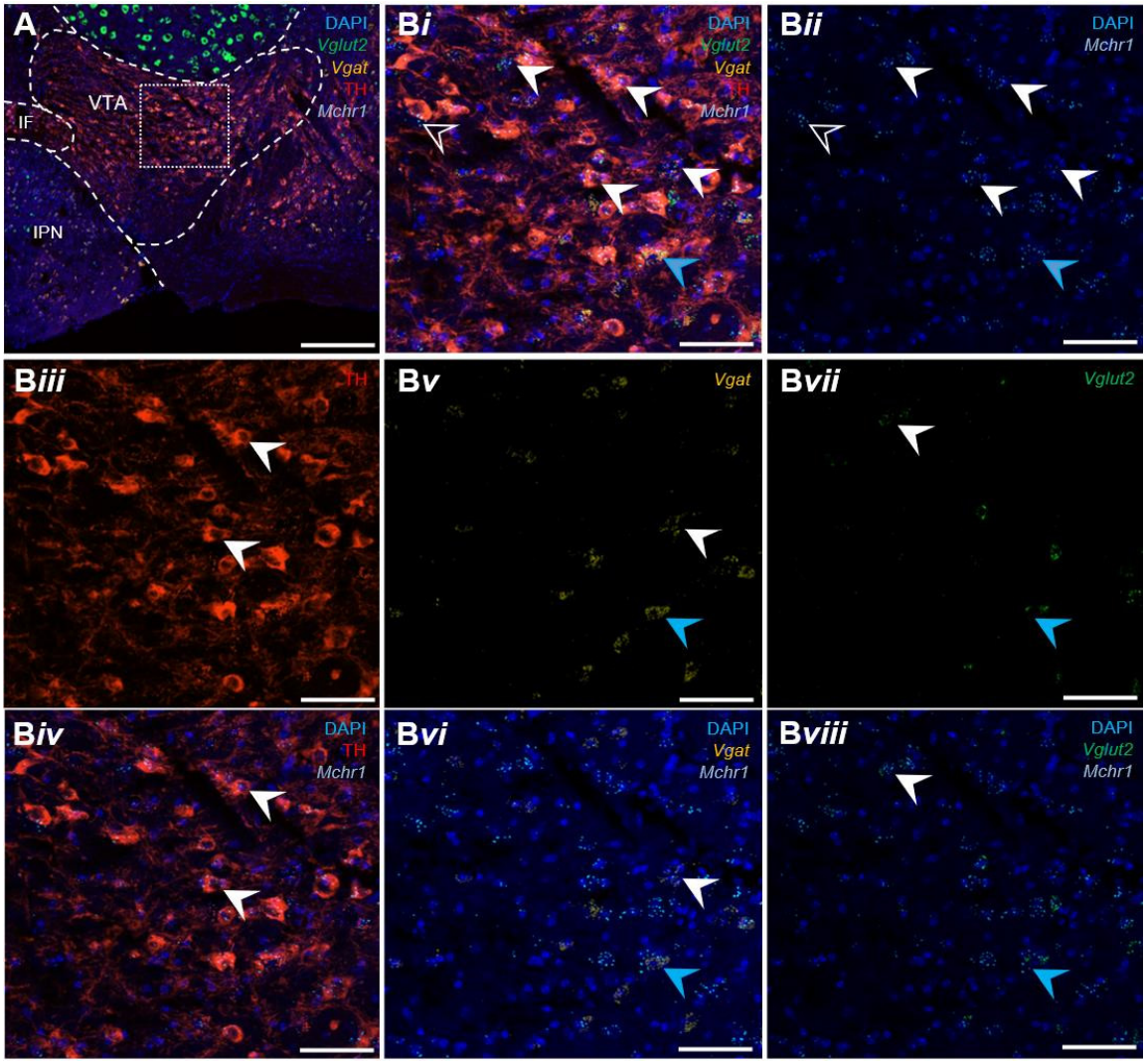

Figure 6. *Mchr1* expression on TH, *Vgat*, *Vglut2* and *Vgat*/*Vglut2* VTA cells. Low (**A**) and high magnification confocal photomicrographs (**Bi–viii**, outlined in **A**) of *Vglut2*, *Vgat*, TH, and *Mchr1* expression in the VTA. *Mchr1* signal (**B*ii***) was observed in TH (**B*iii***, **B*iv***), *Vgat* (**B*v***, **B*vi*** *),* and *Vglut2* (**B*vii***, **B*viii***) cells (white arrowhead), cells expressing *Vgat* and *Vglut2* (blue arrowhead), and cells lacking TH, *Vgat*, and *Vglut2* (open arrowhead) are all observed in the VTA. Scale bars: **A**, 250 µm; **B**, 50 µm. IF, interfascicular nucleus raphe; IPN interpeduncular nucleus; VTA, ventral tegmental area.

4.1.5 Quantification and Distribution of TH, *Vgat*, *Vglut2* and *Vgat*/*Vglut2* with *Mchr1* in the VTA

TH, *Vgat*, *Vglut2*, and *Vgat*/*Vglut2* VTA cell populations were quantified and mapped to their corresponding ARA Level (L) to assess the distribution pattern of each cell type.

TH cells are found sparingly in the anterior levels of the VTA (Figure 7A, B), become much more abundant in the middle of the VTA (L84–87; Figure 7C–E), and dwindle in number toward the posterior section of the VTA (Figure 7F, G). Interestingly, TH neurons tend to be more abundant near the ventral border of the VTA compared to the more dorsal portions of the region (Figure 7C, D, E). Across all levels, *Mchr1* colocalization with TH appears most concentrated in these more ventral clusters of TH neurons (Figure 7C, D, E). Examining the VTA as a whole, a large proportion (78.8 ± 9.8%, n = 3) of TH cells also express *Mchr1* (Figure 7H). The proportion of TH neurons that express *Mchr1* is consistently high (> 50% at each ARA level) throughout the VTA (Figure 7H). Interestingly, *Mchr1* expression appeared the most concentrated in the ventral clusters of TH neurons, with L86 and 87 showing the densest expression of *Mchr1*+ TH cells in these areas (Figure 7D, E).

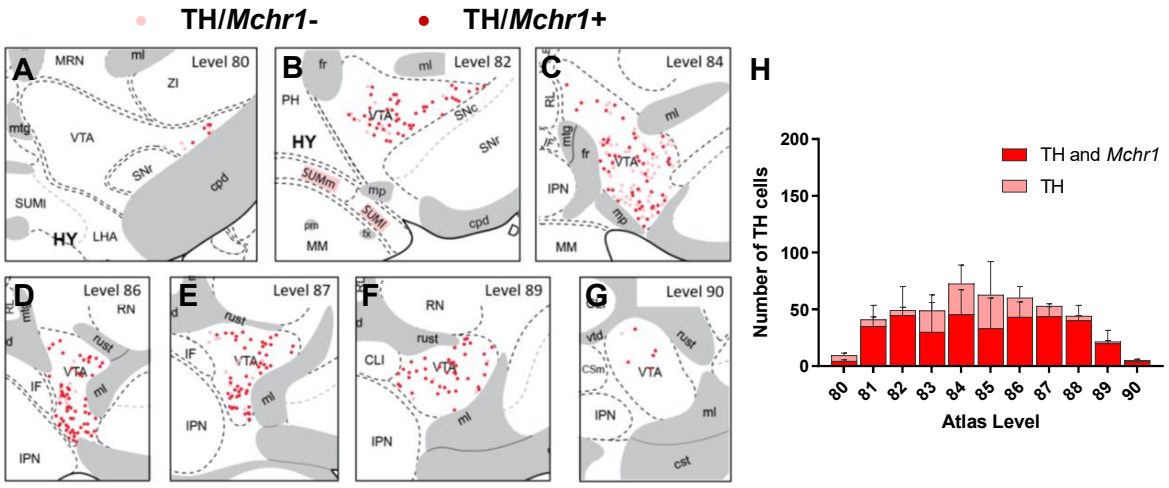

Figure 7. Distribution and quantification of TH neurons expressing *Mchr1* in the VTA. Coronal maps of TH neurons throughout the anteroposterior extent of the VTA that show the presence (red dots) or absence (pink dots) of *Mchr1* (**A–G**). Number of TH neurons expressing *Mchr1* and without *Mchr1* is quantified throughout the VTA at each ARA level (n = 3; **H**).

Consistently abundant expression of *Vgat* cells is observed throughout the anteroposterior span of the VTA (Figure 8A–G). Although the expression is similar throughout, the VTA occupies a smaller space in the posterior levels compared to anterior portion and so expression of *Vgat* neurons appears more dense in the posterior extremes of the region (L89 and 90; Figure 8F, G). No consistent pattern of expression reveals itself when examining the spatial distribution along the mediolateral and dorsoventral axes, with *Vgat* neurons being widely distributed throughout the space of the VTA. Colocalization of *Mchr1* with *Vgat* is sparse and sporadically distributed on most levels of the VTA (Figure 8A–G). There is a notable cluster of *Mchr1*+ *Vgat* cells that appears in the posterior VTA (L89 and 90; Figure 8F, G). The *Vgat* population shows a consistently low proportion of cells expressing *Mchr1* (rarely approaching or surpassing 50% on each level; Figure 8H). Overall, 38% (38.1 ± 3.5%, n = 3) of *Vgat* cells were found to express *Mchr1* (Figure 8H).

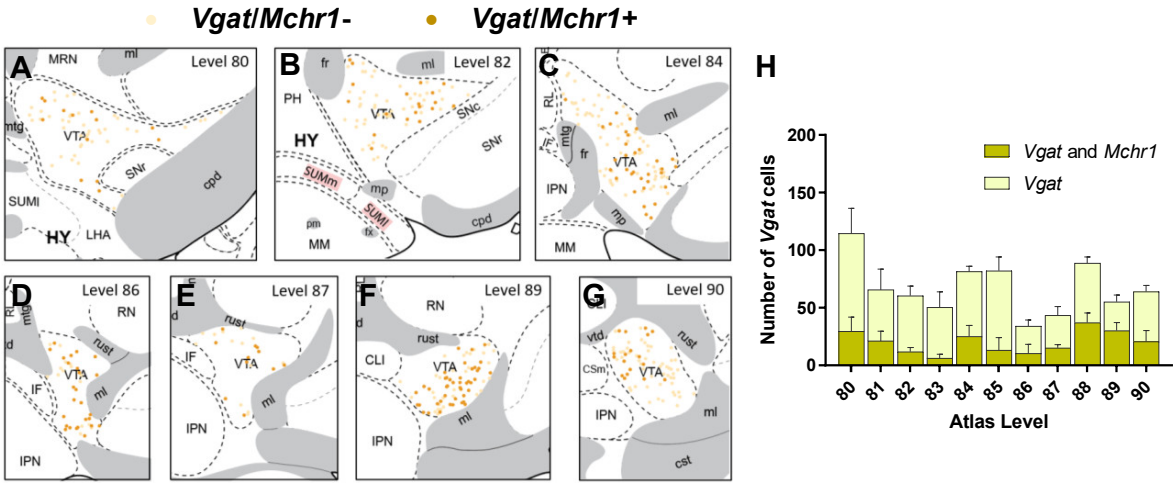

Figure 8. Distribution and quantification of *Vgat* neurons expressing *Mchr1* in the VTA. Coronal maps of *Vgat* neurons throughout the anteroposterior extent of the VTA that show the presence (dark yellow dots) or absence (light yellow dots) of *Mchr1* (**A–G**). Number of *Vgat* neurons expressing *Mchr1* and without *Mchr1* is quantified throughout the VTA (n = 3; **H**).

A high abundance of *Vglut2* cells is observed in the anterior VTA (L80–84; Figure 9A–C) while much less are observed in the levels posterior to this position (Figure 9D–G). *Vglut2* expression appears more concentrated toward the medial border of the VTA compared to the lateral border (Figure 9A–F). Examining the dorsoventral distribution, there are generally fewer *Vglut2* cells near the ventral border of the VTA compared to the dorsal (Figure 9C–F). *Vglut2* cells predominantly show *Mchr1* expression in the anterior most VTA, specifically Level 80 (Figure 9A, H). Interestingly, although few in number, most *Vglut2* cells in the posterior half of the VTA (L86–90; Figure 9D–H) express *Mchr1*. About 50% of *Vglut2* cells on any given level express *Mchr1* (Figure 9H). Perhaps unsurprisingly, the observation that each level has roughly 50% of *Vglut2* cells express *Mchr1* is reflected when examining the VTA as a whole, as 54% (54.1 ± 5.0%, n = 3) of *Vglut2* neurons in the VTA are *Mchr1*+ (Figure 9H).

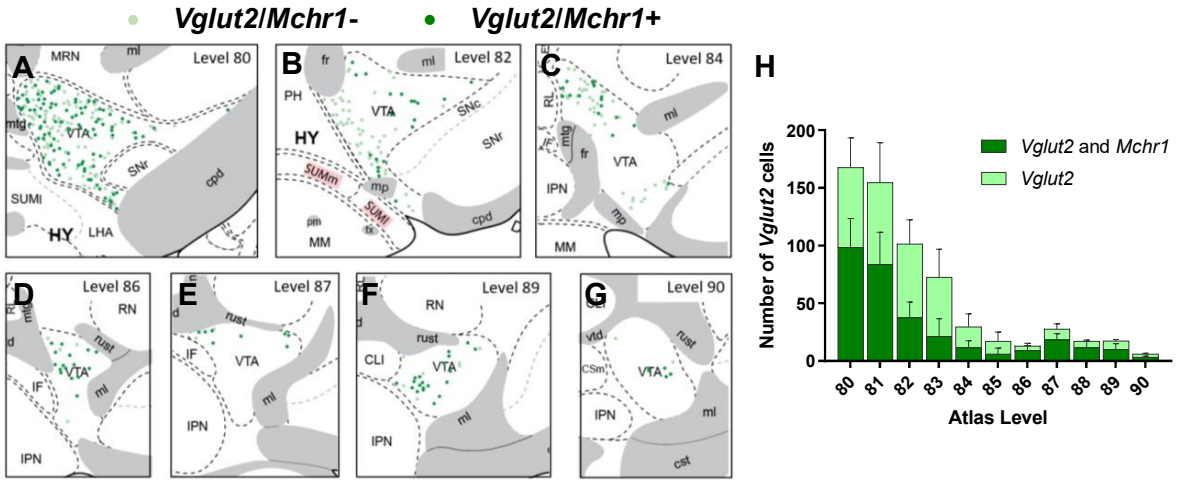

Figure 9. Distribution and quantification of *Vglut2* neurons expressing *Mchr1* in the VTA. Coronal maps of *Vglut2* neurons throughout the anteroposterior extent of the VTA that show the presence (dark green dots) or absence (light green dots) of *Mchr1* (**A–G**). Number of *Vglut* neurons expressing *Mchr1* and without *Mchr1* is quantified throughout the VTA (n = 3; **H**).

Vgat/*Vglut2* cells are consistently observed throughout the anteroposterior span of the VTA (Figure 10A–G) in similar numbers (Figure 10H). Pockets of a slightly higher number of *Vgat/Vglut2* are observed in the middle and posterior VTA (L84, 86, and 90; Figure 10C, D, G) but the number of *Vgat*/*Vglut2* neurons remains low and never exceeds 50 (Figure 10H). These cells appear more abundant in the dorsal VTA with few toward the ventral border (Figure 10A–G). *Mchr1* expression is consistently observed in above 33% of *Vgat*/*Vglut2* cells throughout this population (Figure 10H) but does appear most concentrated in levels with a higher number of *Vgat*/*Vglut2* cells (L86 and 90; Figure 10D,G). Taken together, over 55% (55.5 ± 1.8%, n = 3) of *Vgat*/*Vglut2* VTA cells are *Mchr1*+ and, interestingly, this cell type shows the least variation in the proportion of cells that express *Mchr1* (Figure 10H).

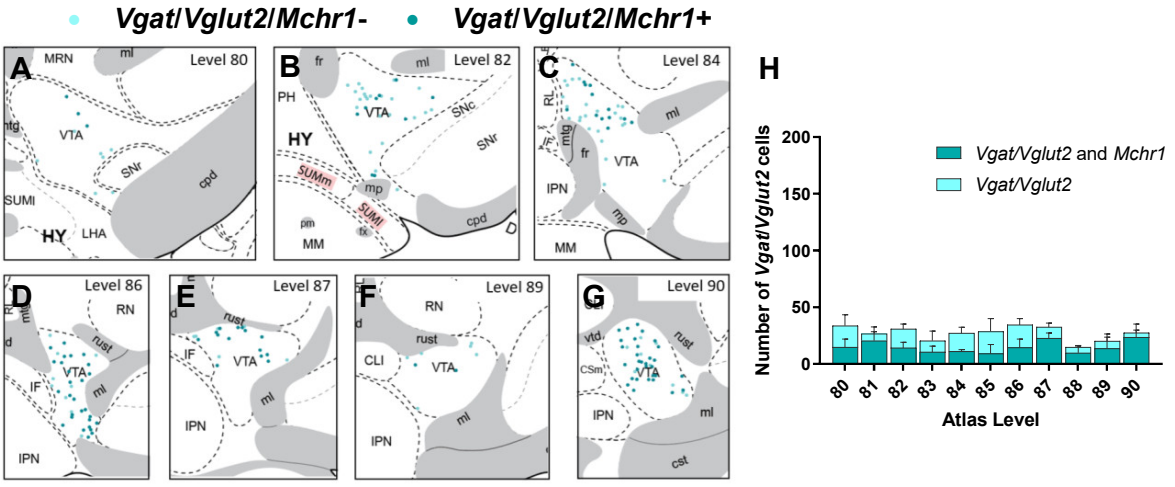

Figure 10. Distribution and quantification of *Vgat*/*Vglut2* neurons expressing *Mchr1* in the VTA. Coronal maps of *Vgat*/*Vglut2* neurons throughout the anteroposterior extent of the VTA that show the presence (dark blue dots) or absence (light blue dots) of *Mchr1* (**A–G**). Number of *Vgat*/*Vglut2* neurons expressing *Mchr1* and without *Mchr1* is quantified throughout the VTA (n = 3; **H**).

4.1.6 Summary of *Mchr1* expression in the VTA

Taken together, we found *Mchr1* expression at all major subtypes of VTA cells, including those that are dopaminergic, GABAergic, glutamatergic, as well as those that are GABAergic and glutamatergic. Interestingly, a large portion (30.1 ± 14.1%, n = 3) of *Mchr1* neurons have yet to be neurochemically defined, as they did not express TH, *Vgat*, or *Vglut2* mRNA (Figure 11). These neuroanatomical results converge upon the expression of *Mchr1* mRNA and MCHR1 protein in major VTA cell types.

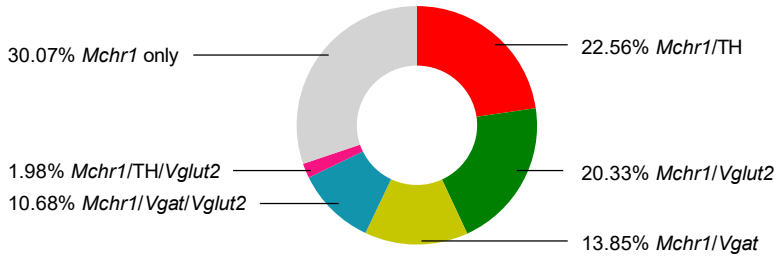

Figure 11. Neurochemical characterization of *Mchr1* VTA neurons. The population of *Mchr1* VTA neurons described in terms of VTA cell-types

4.2 MCH neurons innervate the VTA

As MCH may act in the VTA, we determined if MCH neurons can innervate VTA cells. We injected a cre-dependent retrograde AAV (AAVrg-flox-hChR2(H134R)-mCherry) into the VTA of male *Mch-cre* mice to determine if retrograde tracing from nerve terminals within the VTA would label MCH cells. We observed neurons in the LHA showing both mCherry and MCH immunoreactivity (Figure 12A,B), thus suggesting that MCH neurons may innervate VTA neurons.

Consistent with this, anterograde tracing using a cre-dependent AAV (AAV(8)-CMV-DIO-Synaptophysin-EYFP) encoding synaptophysin-EYFP into the LHA of *Mch-cre* mice revealed EYFP expression within the VTA (Figure 13A). Furthermore, some, though not all, EYFP-immunoreactive fibers colocalized with MCH immunoreactivity in the VTA (Figure 13B, C).

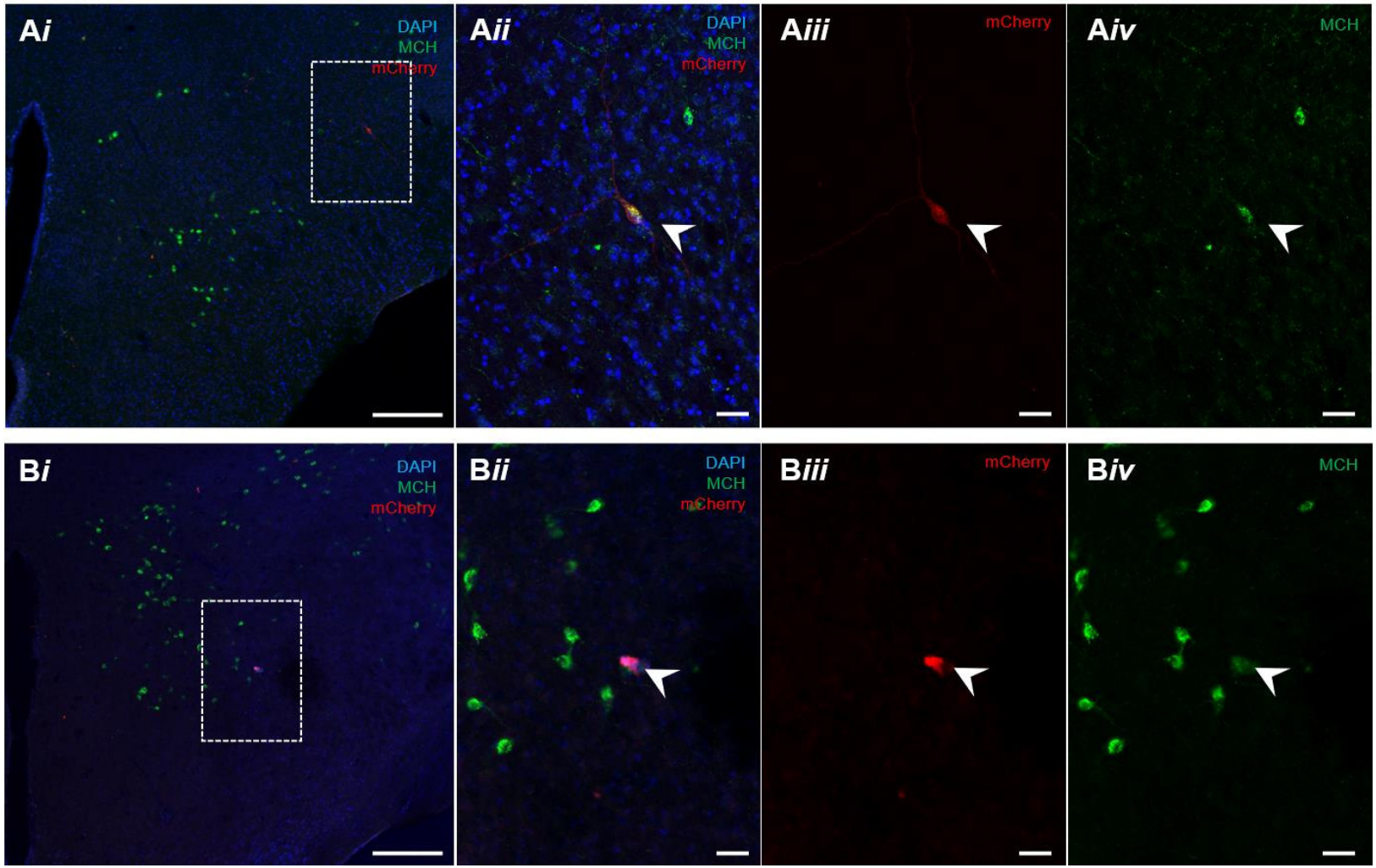

Figure 12. MCH neurons innervate the VTA. Confocal photomicrographs showing mCherry and MCH immunoreactivity, counterstained with DAPI, in the lateral hypothalamus of *Mch-cre* mice following injection of a cre-dependent retrograde virus (AAV flox-hChR2(H134R)-mCherry-WPRE-HGHpA) into the VTA (**A** and **B**). Representative MCH neurons lateral (**A**) and medial (**B**) of the fornix expressing mCherry at low (***i***) and high (***ii–iv***) magnification. Scale bars: ***i,*** 250 µm; ***ii-iv***, 30 µm.

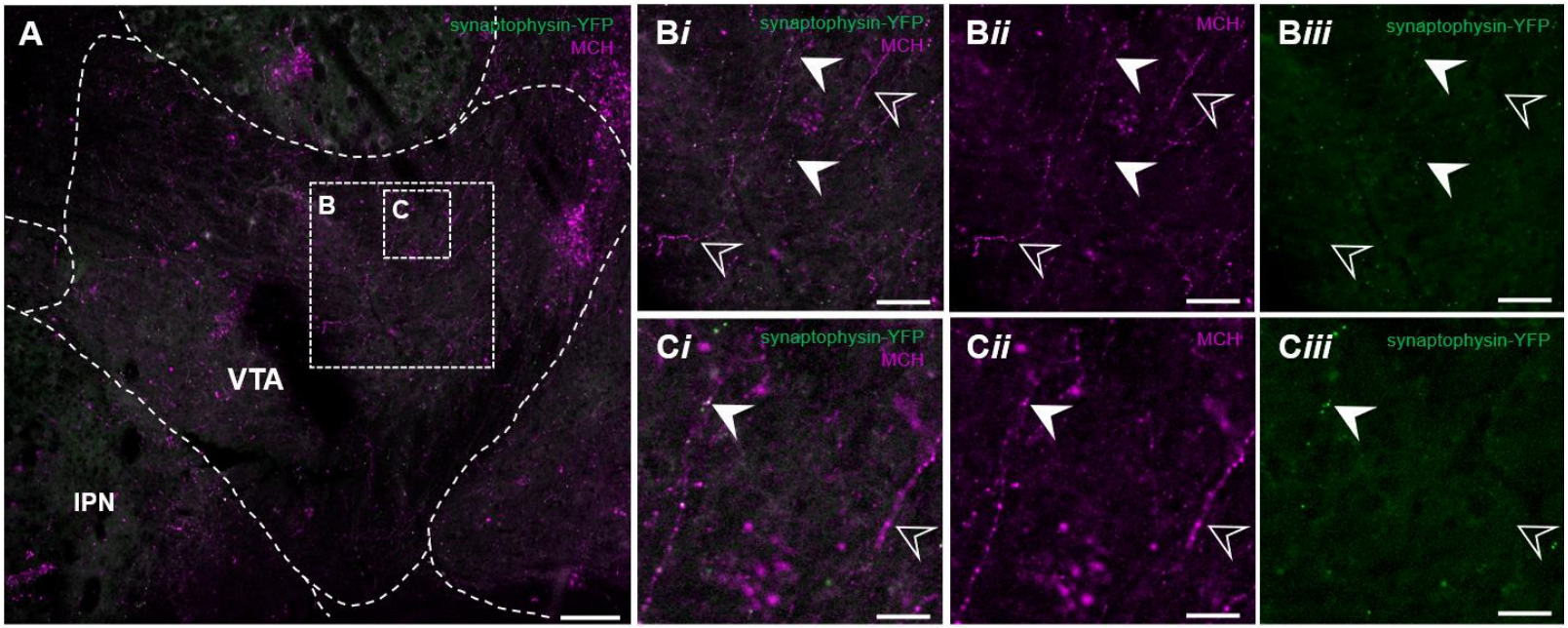

Figure 13. **MCH immunoreactivity along nerve fibers and terminals within the VTA.** Confocal photomicrographs showing EYFP and MCH immunoreactivity in the VTA of mice following injection of a cre-dependent anterograde virus (AAV(8)-CMV-DIO-Synaptophysin-EYFP) into the LHA (**A**). Low (**B**) and high (**C**) magnification images of representative MCH fibers showing the presence (filled arrowheads) or absence (open arrowheads) of EFYP. Scale bars: **A**, 100 µm; **B, 50** µm; **C**, 20 µm. IPN interpeduncular nucleus; VTA, ventral tegmental area.

4.3 MCH regulated dopaminergic, GABAergic, and glutamatergic cells in the VTA

We have shown that MCH neurons project to the VTA (**Section 4.2**) and that the major VTA cell types express MCHR1 (**Section 4.1**). Here, we performed whole-cell patch-clamp recordings to establish whether MCH can act directly within the VTA to regulate the activity of dopaminergic, GABAergic, or glutamatergic VTA cells in acute brain slices from *Th-cre;L10-Egfp*, *Vgat-cre;L10-Egfp*, or *Vglut2-cre;L10-Egfp* reporter mice.

4.3.1 MCH directly hyperpolarized *Th* and *Vgat* VTA neurons

Bath application of 3 μM MCH reversibly hyperpolarized (−4.2 ± 0.9 mV, n = 6) about 38% (6 of 16 cells) of *Th-cre;L10-Egfp* neurons in the VTA (Figure 14A). The peak effect of MCH appeared within 10 minutes of bath application, was long-lasting, and persisted for at least 25 min before returning to its resting membrane potential.

We then assessed if MCH-mediated inhibition of *Th* VTA cells was activity-dependent by determining if the hyperpolarizing effect of MCH would persist if the cell was pretreated with the voltage-gated sodium channel blocker tetrodotoxin (TTX). However, as the effect of bath-applied MCH (5–6 min) is so long-lasting, we first established whether a short (5–10 s) puff application of MCH could similarly hyperpolarize *Th* VTA cells but allow more rapid recovery of the resting membrane potential. Puff application of MCH (Figure 14B) produced a sharp membrane hyperpolarization (−7.4 ± 1.4 mV, n = 4) that peaked within 10 seconds and returned to baseline within 40 seconds (Figure 14C*i*). A second puff of MCH applied 3–5 minutes later showed no significant difference in the amplitude of membrane hyperpolarization (−6.2 ± 1.5 mV, n = 4; p = 0.301; Figure

14C*i* and *ii*). No change in membrane potential was observed with a puff of ACSF (1.9 ± 0.4 mV, n = 3; Figure 14C*i* and *ii*). Taken together, we determined that puff-applied MCH enabled a short time course but reproducible membrane hyperpolarization. We thus puff-applied MCH to a *Th-cre;L10-Egfp* VTA cell and then pretreated the cells with 500 nM TTX. Interestingly, the MCH-mediated hyperpolarization (−6.1 ± 1.5 mV, n = 5) persisted in the presence of TTX (−4.8 ± 1.1 mV, n = 5; p = 0.460; Figure 14C*iii* and *iv*). These findings indicate that MCH directly hyperpolarized *Th* VTA cells.

Bath applied MCH also reversibly hyperpolarized GABAergic VTA neurons (−4.8 ± 2.4 mV, n=5; Figure 15A) in acute brain slices from *Vgat-cre;L10-Egfp* mice. This effect was observed in 36% of *Vgat-cre;L10-Egfp* cells (5 of 14 cells) and was also long-lasting, with a washout after 25 min (Figure 15A). In a new subset of *Vgat-cre;L10-Egfp* cells, we determined that the MCH-mediated hyperpolarization (−2.5 ± 1.0 mV, n = 4) delivered by puff application persisted following TTX pre-treatment (−1.5 ± 0.8 mV, n = 4; p = 0.200; Figure 15B*i*, B*ii*).

By contrast, MCH application did not change the resting membrane potential of glutamatergic VTA cells in slices from *Vglut2-cre;L10-Egfp* mice (0/10 cells).

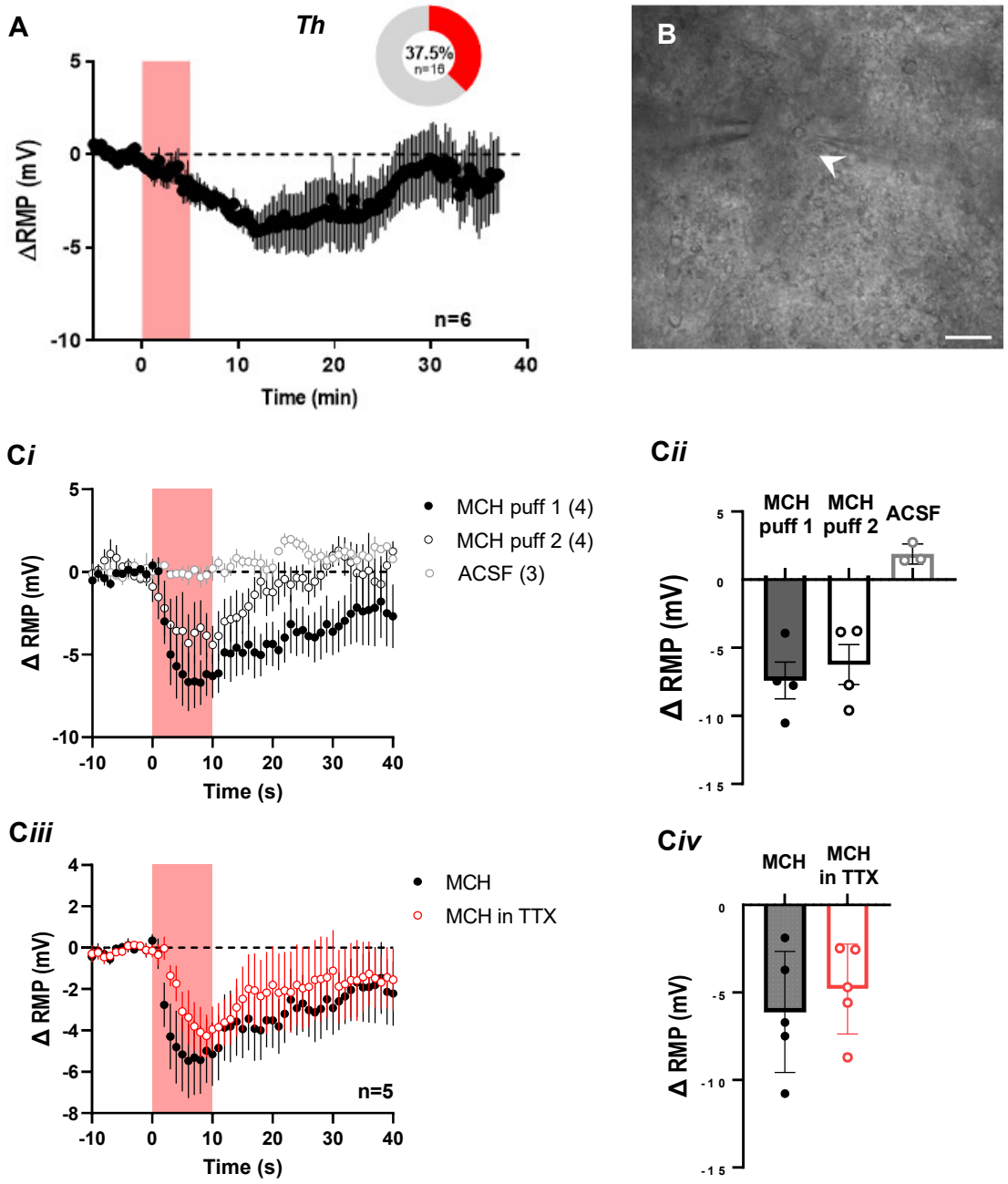

Figure 14. **MCH directly hyperpolarizes *Th* VTA neurons.** Time course of change in RMP (Δ RMP) relative to the baseline period prior to 3 μM MCH application in *Th* neurons with donut chart showing the proportion of *Th* cells that were MCH-responsive (**A**). A second pipette was positioned 20 μm next to patched cells to allow puff application of MCH or ACSF(**B**). Time course of Δ RMP showing puff applications of: 3 μM MCH and ACSF onto *Th* neurons (**C*i***) with peak effect of each puff (**C*ii***); MCH onto *Th* neurons in the absence and presence of 500 nM TTX (**C*iii***) with peak effect of each treatment (**C*iv***). Scale bar; 20 μm.

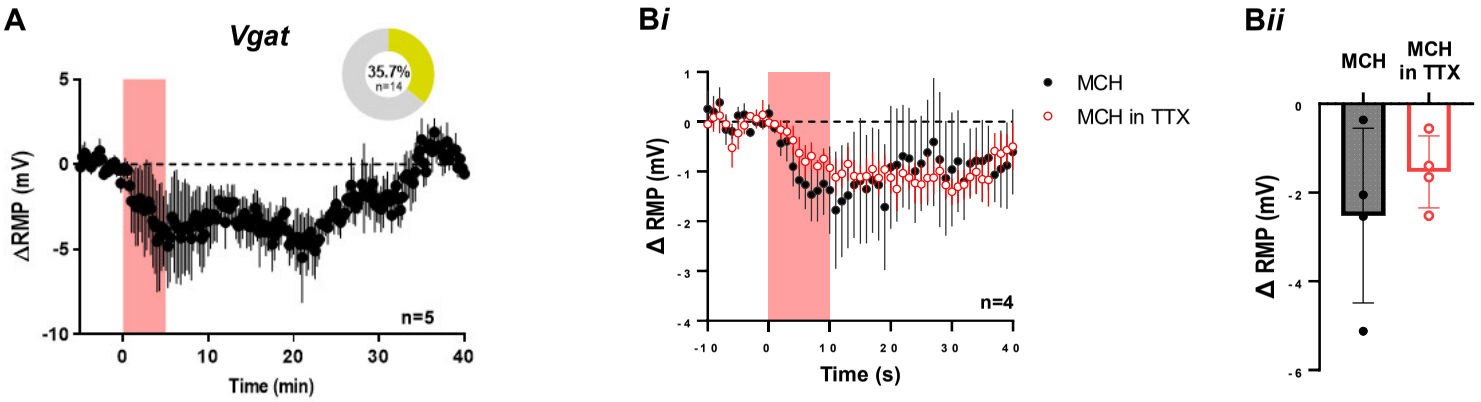

Figure 15. **MCH directly hyperpolarizes *Vgat* VTA neurons.** Time course of Δ RMP relative baseline prior to 3 μM MCH application in *Vgat* neurons with donut chart showing the proportion of *Vgat* cells that were MCH-responsive (**A**). Time course of Δ RMP showing puff applications of 3 μM MCH onto *Vgat* neurons in the absence and presence of 500 nM TTX (**B*i***) with peak effect of each treatment (**B*ii***).

4.3.2 MCH modulated synaptic inputs to *Th* and *Vglut2* VTA neurons

As VTA dopaminergic output can be regulated by the local glutamatergic and GABAergic circuitry (Bariselli et al., 2016; Morales & Margolis, 2017; Wang et al., 2015), we assessed if MCH regulates the glutamatergic and/or GABAergic input to *Th* VTA cells. Bath application of 3 μM MCH produced a delayed 1.6 ± 0.6 Hz (n = 8) increase in sEPSC frequency at *Th-cre;L10-Egfp* VTA neurons, where the peak effect was seen 25 min after MCH application (Figure 16A). In the event that this delayed increase was not MCH-dependent, we performed control recordings where ACSF was bath applied, but in the absence of MCH, and found that ACSF alone did not alter sEPSC frequency (Figure 16A). By contrast, bath application of MCH did not impact sIPSC frequency at *Th-cre;L10-Egfp* neurons (Figure 16B).

As MCHR1 is an inhibitory G-protein coupled receptor, we assessed if the MCH-mediated glutamatergic drive at *Th* cells may be ascribed to an inhibition of upstream GABAergic input to *Vglut2-cre;L10-Egfp* VTA cells. Bath application of 3 μM MCH decreased the frequency of sIPSC events at *Vglut2* cells (−0.7 ± 0.3Hz; Figure 16C). Taken together, these findings suggest that in addition to directly inhibiting *Th* cells, MCH may engage a local disynaptic circuit between *Vgat*, *Vglut2*, and *Th* VTA neurons to regulate output from the VTA (Figure 16D).

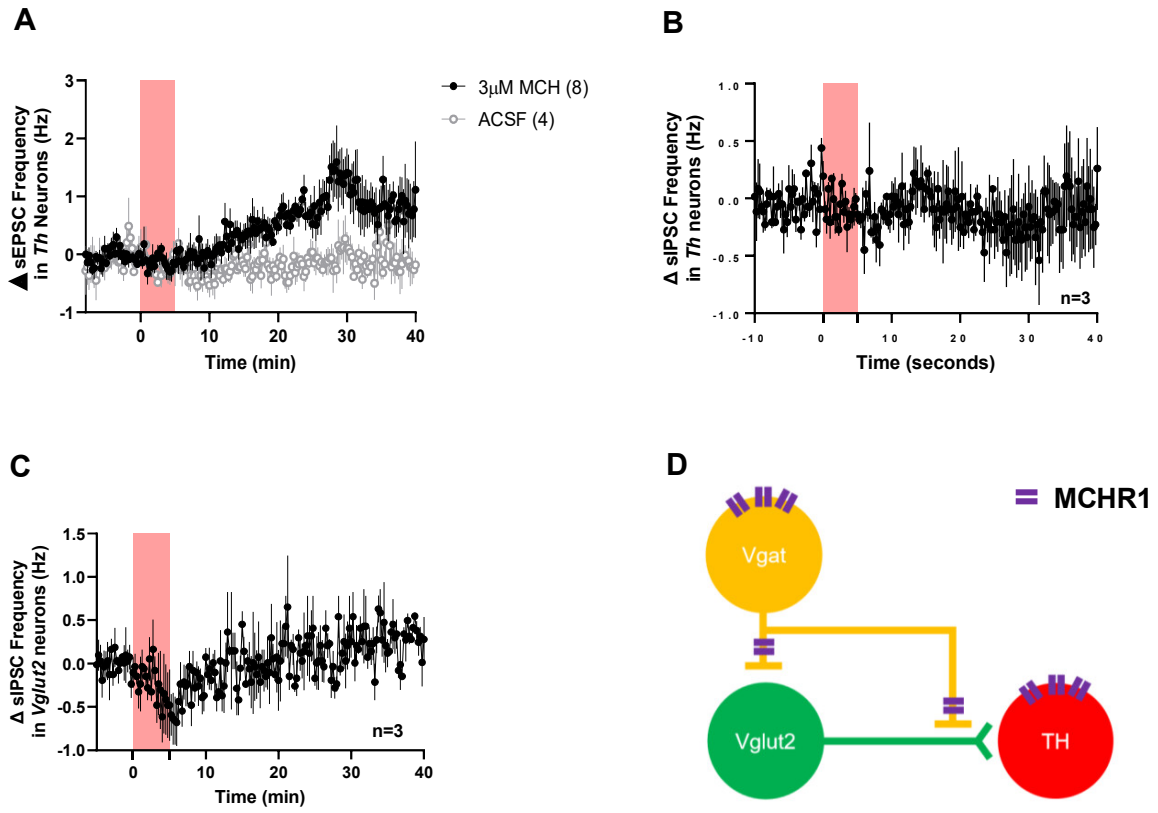

Figure 16. **MCH application alters synaptic inputs to *Th* and *Vglut2* VTA neurons.** Change in sEPSC (Δ sEPSC) frequency relative to baseline period prior to 3 μM MCH (red) or ACSF (black) application in *Th* neurons (**A**). Change in sIPSC (Δ sIPSC) frequency relative to baseline prior to 3 μM MCH application in *Th* neurons (**B**). Time course of Δ sIPSC frequency relative to baseline prior to 3 μM MCH application in *Vglut2* neurons (**C**). Model of potential local disynaptic pathway between *Vgat*, *Vglut2*, and *Th* VTA neurons (**D**).

5. Discussion

MCH can inhibit DA release (Chee et al., 2019), thus the loss of MCH (Mul et al., 2011; Pissios et al., 2008) or its receptor (Chee et al., 2019) leads to a hyperdopaminergic state, which is marked by pronounced hyper-locomotor activity. While the VTA contributes the most abundant source of DA in this system, *Mchr1* mRNA has not been previously detected in the mouse VTA (Chee et al., 2013) despite detection of the MCHR1 protein (Diniz et al., 2020), so it was not clear that the VTA could be a target site of MCH action. This present study provided the neuroanatomical basis for MCH action in the mouse VTA. We showed that the mouse VTA contains *Mchr1* mRNA and expresses functional MCHR1 protein on at least two major subpopulations of VTA neurons. We found MCH-immunoreactive fibers that were in proximity to synaptophysin nerve terminals, so MCH can be transported and released in the VTA. Importantly, we demonstrated that functional MCHR1 activation in the VTA can mediate direct or indirect mechanisms to regulate dopaminergic VTA cells.

5.1 Abundance and sex differences in *Mchr1* mRNA and MCHR1 protein expression

The level of *Mchr1* mRNA in the rat VTA is comparable to that in the hypothalamus and hippocampus (Hervieu et al., 2000; Saito et al., 2001). This relative expression pattern of *Mchr1* mRNA was also seen here in the mouse brain. While *Mchr1* expression in the mouse VTA was lower than that seen in the striatum, which comprises the highest level of *Mchr1* mRNA in the brain, it was similar to that in the hypothalamus and

hippocampus, where MCHR1 has been implicated in food and water intake (Abbott et al., 2003; Chee et al., 2013; Clegg et al., 2003) and cognition (Pachoud et al., 2010), respectively.

Interestingly, there was a sex difference in *Mchr1* expression, which was nearly two-fold higher in the VTA of female mice. This difference may account for the pronounced hyperactivity seen following *Mchr1* deletion in female mice (Chee et al., 2019). However, this sex difference in *Mchr1* gene expression may not reflect a difference in MCHR1 protein expression within the VTA (Diniz et al., 2020). MCHR1 protein is concentrated on the primary cilia of neurons within the brain, and this includes the VTA (Diniz et al., 2020). Our findings affirmed the expression of MCHR1 protein on the cilia of VTA neurons, including in the VTA of both male and female mice, but the relative abundance of MCHR1 protein has not yet been quantified.

5.2 MCHR1 expression in major subpopulations of VTA cells

5.2.1 Distribution of *Mchr1* in dopaminergic VTA neurons

The majority of dopaminergic VTA neurons express *Mchr1*. Dopaminergic VTA cells are commonly associated with reinforcement of learning cues, habit formation, and predicted reward values (Schultz et al., 1997; Schultz, 2002; Wise, 2004). Additionally, DA cells of the VTA have been shown to drive motivated or effortful behaviours to obtain predicted reward from, among others things, social interaction, drugs of abuse, and food (Gunaydin et al., 2014; Salamone & Correa, 2012; Schultz, 2002; Wise, 2004). DA neuron activity is implicated in addiction to drugs of abuse (Schultz, 2002; Volkow & Wise, 2005; Wise, 2004) and has been suggested to play a similar role in the reward

and motivation driving feeding in obesogenic phenotypes (Volkow & Wise, 2005; Wise, 2006). In line with this, it has been shown that DA VTA projections to the NAcc contribute to the rewarding and motivational aspects of hedonic feeding (Wise, 2006). Interestingly, loss of MCH signalling has been shown to impact DA signalling, producing a hyperdopaminergic state that underlies an increase in locomotor activity and energy expenditure (Chee et al., 2019). However, it is not known if MCH acts at the level of the VTA to elicit this effect. We found that *Mchr1* is expressed in most TH neurons throughout the anteroposterior span of the VTA. We show TH neurons were concentrated in the mid-section of the VTA with little expression toward the anterior and posterior extremes of the VTA. This is consistent with previous studies examining TH expression in the VTA (Morales & Root, 2014; Morales & Margolis, 2017; Yamaguchi et al., 2011). This high prevalence of *Mchr1* expression on TH suggests this population could be a target of MCH action and provides a potential direct method by which MCH could act to inhibit DA release within the NAcc.

5.2.2 Distribution of *Mchr1* in GABAergic VTA neurons

The observation of a GABAergic cluster of cells in the posterior VTA is consistent with findings in rats and mice, where the tail of the VTA (tVTA) shows high expression of GABAergic neurons (Barrot et al., 2012; Bouarab et al., 2019; Jhou, 2021; Sanchez-Catalan et al., 2014). Interestingly, the tVTA shows dense GABAergic projections to other VTA neurons (Barrot et al., 2012; Jhou et al., 2009; Lecca et al., 2012) and has been shown to provide functionally relevant inhibitory tone to DA VTA neurons (Barrot et al., 2012; Bouarab et al., 2019; Guan et al., 2012). The posterior VTA is functionally

different from the anterior VTA, as GABA neurons showing different basal physiological properties (Polter et al., 2018; Simmons et al., 2017), gene expression (Lahti et al., 2016), and responsiveness to cannabinoids and opioids (Barrot et al., 2012; Sanchez-Catalan et al., 2014). The tVTA has also been implicated in responsiveness to alcohol. RAts will self administer ethanol to the posterior but not anterior VTA (Guan et al., 2012). Interestingly, alcohol-induced conditioned place preference is decreased with MCHR1 deletion (Karlsson et al., 2016) and MCHR1 blockade decreases self-administration of alcohol (Cippitelli et al., 2010). Furthermore, exposure to alcohol has been shown to stimulate tVTA DA cells but suppress anterior DA VTA neurons (Guan et al., 2012).

In light of these findings, it is interesting that we observe a dense cluster of *Vgat* neurons in the posterior VTA and that this cluster shows the highest proportion of *Mchr1*+ cells within the VTA *Vgat* population. GABAergic neurons in the VTA were most prominent in the caudal or tail of the VTA. However, compared to the TH VTA population, a smaller portion of *Vgat* VTA neurons (<40%) expressed *Mchr1*. Although the number of *Vgat* cells is not particularly high in the posterior VTA, the proportion of *Vgat* cells showing *Mchr1* expression is highest in these later levels. Additionally, the smaller size of the VTA and decreased presence of other VTA cell types emphasize the density of *Mchr1*+ *Vgat* neurons in these levels. This supports that the posterior VTA is anatomically and functionally different in mice and suggests this subregion as a site of MCH action at GABAergic cells. As well, the expression of *Mchr1* in *Vgat* VTA neurons is consistent with findings by Chee et al. (2019) demonstrating GABAergic circuitry underlies MCHR1 activation.

5.2.3 Distribution of *Mchr1* in glutamatergic VTA neurons

Over half of *Vglut2* VTA neurons identified expressed *Mchr1.* Glutamatergic VTA cells have been shown to drive DA release by VTA DA neurons and promote conditioned place preference (Wang et al., 2015). Additionally, glutamate cells themselves have been shown to signal both reward and aversion predictions (Cai & Tong, 2022). Activation of glutamatergic neurons has been shown to drive preference independent of DA (Zell et al., 2020) but sustained activation can result in avoidance behaviours (Yoo et al., 2016). The apparent contradicting effects of glutamatergic VTA neurons could be due to different subpopulations within the VTA (Cai & Tong, 2022). Additionally, *Vglut2* neurons have been shown to make local synapses with dopaminergic and non-dopaminergic VTA neurons (Dobi et al., 2010), suggesting GABA interneurons may contribute to the apparent contradicting roles of glutamatergic VTA neurons (Cai & Tong, 2022). We show *Vglut2* neurons are much more abundant in the anterior VTA and quickly decreased in number through most of the VTA. *Vglut2* expression and distribution is consistent with previously reported findings for *Vglut2* expression and distribution in the VTA (Morales & Root, 2014; Root et al., 2018; Yamaguchi et al., 2007). Interestingly, the proportion of *Vglut2* cells that expressed *Mchr1* was very steady throughout the VTA regardless of the number of *Vglut2* cells. This resulted in a large cluster of *Vglut2*/*Mchr1* neurons in the anterior VTA and a small number of sporadically distributed cells throughout the mid- and posterior sections. In combination with the distribution of VTA cell types, this neuroanatomical distinction could be indicative of local circuitry and contribute to the seemingly opposing functions of VTA glutamate cells (Cai & Tong, 2022).

5.2.4 Coexpression of multiple chemical messengers in the VTA

Vgat/*Vglut2* neurons were the only major population of cells we observed expressing a combination of TH, *Vgat*, and *Vglut2*. This population shows characteristics of both *Vgat* and *Vglut2* neurons, signaling both rewarding and aversive outcomes (Root et al., 2020). The presence of *Vgat*/*Vglut2* cells throughout the VTA is consistent with findings demonstrating that there is a population of VTA neurons that corelease GABA and glutamate (Root, Mejias-Aponte, Zhang, et al., 2014) and express both *Vgat* and *Vglut2* (Root et al., 2018).

VTA neurons may also be both glutamatergic and dopaminergic (Morales & Root, 2014; Morales & Margolis, 2017; Yamaguchi et al., 2011), however we have not detected high colocalization between TH and *Vglut2*. Based on the ARA definition of the VTA, we did not expect to see a large number of TH/*Vglut2* as we performed our analyses based on the neuroanatomical boundaries defined by the ARA (Dong, 2008) for mice. In rats, the boundaries of the VTA can include the medial space between the left and right VTA to encompass the interfascicular nucleus raphe, rostral linear nucleus raphe, and central linear nucleus raphe as subregions of the VTA (Morales & Root, 2014; Morales & Margolis, 2017; Yamaguchi et al., 2011). As shown by Yamaguchi et al., (2011), most neurons that express TH and *Vglut2* are observed close to the midline and as our analyses did not include these areas, it is not surprising we did not observe a large number of TH/*Vglut2* cells.

Although VTA cells co-releasing TH and GABA have been identified (Stamatakis et al., 2013; Tritsch et al., 2012), cells expressing TH and *Vgat* have not been observed and

our results support that this is not a substantial population within the VTA. These results are reconciled with the corelease of TH and GABA by findings showing that GABA release may not be dependent on VGAT in the VTA and that the vesicular monoamine transporter 2 (VMAT2) can fully support GABA release from dopaminergic cells (Tritsch et al., 2012). Expression of other markers of GABAergic cells such as VMAT2 and glutamate decarboxylase (GAD) should be explored in future studies to examine if there are differences in the distribution of GABAergic subtypes of the VTA and to determine if *Mchr1* is preferentially expressed in a certain subset of GABA cells.

5.2.5 Limitations

As Mchr1 expression may be higher in female than male mice, it would be important to determine how the distribution of *Mchr1* is in different VTA cell types differs between male and female mice. Differential expression of *Mchr1* on a distinct subpopulation of VTA cells may also implicate sex differences in MCH-mediated behaviors.

5.3 Projections from MCH neurons to the VTA

MCH neurons have widespread projections throughout the brain. Our results show that MCH neurons also project to the VTA. MCH-immunoreactive fibers within the VTA slice illustrated that there is the capacity for MCH to be transported to the VTA. Furthermore, some punctate MCHR1-immunopositive labeling are also colocalized with or in immediate proximity to synaptophysin-labeled nerve terminals, thus implicating putative MCH release sites. These findings suggest that MCH neurons may be able to act via short range and long-range transmission within the VTA. This is consistent with findings

demonstrating short range release (del Cid-Pellitero & Jones, 2012) and volume transmission (Noble et al., 2018) of MCH. Additionally, consistent with findings showing MCH afferents to the VTA (Faget et al., 2016), we show retrograde evidence that MCH neurons innervate VTA cells, further supporting that there is the capacity for MCH to be released in the VTA.

5.4 MCH-mediated regulation of DA release

5.4.1 Direct inhibition of dopaminergic VTA neurons

MCHR1 is a Gi protein coupled receptor and has known inhibitory actions (Chambers et al., 1999; Hawes et al., 2000; Lembo et al., 1999; Saito et al., 1999). We show that MCH directly hyperpolarized dopaminergic neurons in the VTA in an activity-independent manner. This is consistent with the expression of MCHR1 protein at the soma of TH VTA cells (Diniz et al., 2020) and also with MCH-mediated hyperpolarization observed at the NAcc (Georgescu et al., 2005) and hypothalamus (Abbott et al., 2003; Wu et al., 2009). Interestingly, MCH only produced a hyperpolarization in approximately 38% of *Th* cells recorded. This was slightly lower than expected as we showed that *Mchr1* is expressed in over 75% of TH neurons. This could be a result of a discrepancy between mRNA and protein expression for either MCHR1 or TH. MCHR1 may not be expressed in all cells expressing *Mchr1* and the same is true for TH. These two possibilities could account for the low rate of MCH-responsiveness in recorded *Th* neurons. Taken together, this suggests that direct MCH-mediated inhibition can suppress DA release (Chee et al., 2019), which we can test by amperometry or voltammetry experiments.

5.4.2 GABAergic disinhibition promotes DA release

Dopaminergic VTA cells receive both local GABAergic and glutamatergic input to mediate aversion (Tan et al., 2012) and place preference (Wang et al., 2015), respectively. MCH had no effect on GABAergic input to *Th* VTA neurons, but it did elicit a delayed increase in glutamatergic input to *Th* VTA cells. VTA *Vglut2* cells have been shown to innervate (Dobi et al., 2010) and regulate the activity of dopaminergic VTA cells (Bariselli et al., 2016; Wang et al., 2015). We did not detect MCH effects on the cell body of *Vglut2* VTA cells, and as MCHR1 activation is typically inhibitory (Chambers et al., 1999; Hawes et al., 2000; Lembo et al., 1999; Saito et al., 1999), we would not expect MCH to increase glutamatergic tone by acting on *Vglut2* cells. Rather, we determined if MCH may recruit glutamatergic afferents by suppressing inhibitory input onto *Vglut2* VTA cells.

MCH directly inhibited GABAergic VTA cells, and we found that MCH also suppressed GABAergic input to *Vglut2* VTA cells. Taken together, these findings suggest that MCH can indirectly regulate dopaminergic VTA neurons via a local GABAergic circuit (Figure 16D). Our findings showing MCH can act directly on *Vgat* VTA neurons, and MCHR1 activation at *Vgat* neurons would disinhibit glutamatergic input to *Th* VTA cells. Future studies may utilise optogenetics-mediated circuit mapping to examine the connectivity of MCH and VTA neurons. Our results suggest that inhibiting the local GABAergic neural circuit in the VTA would restore DA levels, for instance following the acute inhibition by MCH directly at *Th* cells. This may be in contrast to prior findings showing that *Mchr1* deletion from *Vgat* cells leads to a hyperdopaminergic state (Chee et al., 2019), but both findings may not be mutually exclusive. Additional recordings from *Th*

VTA cells to assess if inhibiting GABAergic tone confers an upregulation of glutamatergic input to *Th* cells would help demonstrate the validity of our model. This may be done by determining if the increase in sEPSC frequency is abolished in the presence of a GABA receptor antagonist such as bicuculline.

5.4.3 Limitations

One limitation of this study is that we could not target *Vgat*/*Vglut2* VTA for recording. In future studies, we can confirm if recorded cells express both *Vgat* and *Vglut2* following patching by performing ISH for *Vgat* and *Vglut2* recorded cells. Alternatively, the methodology established by Root et al. (Root et al., 2020) and Miranda-Barrientos et al. (Miranda-Barrientos et al., 2021) for targeting this population using a combination of *Cre* and *Flp* viruses would allow for us to assess MCH action specifically at *Vgat*/*Vglut2* VTA cells. However, as we did not have a way of distinguishing *Vgat*/*Vglut2* from all *Vglut2-cre;L10-Egfp* cells, our finding that MCH does not hyperpolarize *Vglut2*+ VTA neurons also demonstrates that *Vgat*/*Vglut2* neurons do not show a change in RMP in response to MCH application. Additionally, effects on RMP and synaptic inputs were observed in both male and female mice, though more animals should be recorded from in order to effectively compare the effects of MCH in male and female VTA cells.

6. Conclusion

MCH can directly regulate local circuitry within the VTA, and it can do so by inhibiting dopaminergic and GABAergic VTA cells. These actions can also recruit glutamatergic afferents within the VTA. Given the higher expression of *Mchr1* in female brains, there may be sex differences in the action of MCH within the VTA. It is already known that *Mchr1* deletion from GABAergic cells mediates a hyperdopaminergic state and it would be of interest to determine if deletion from dopaminergic cells would produce the same effect.

7. References

Abbott, C. R., Kennedy, A. R., Wren, A. M., Rossi, M., Murphy, K. G., Seal, L. J., Todd, J. F., Ghatei, M. A., Small, C. J., & Bloom, S. R. (2003). Identification of hypothalamic nuclei involved in the orexigenic effect of melanin-concentrating hormone. *Endocrinology*, *144*(9), 3943–3949. https://doi.org/10.1210/en.2003-0149

Advanced Cell Diagnostic. (2019). *RNAscope® Multiplex Fluorescent Reagent Kit v2 Assay - With Sample Preparation and Pretreatment*. *323100*.

Advanced Cell Diagnostics. (2020). *RNAscope ® Multiplex Fluorescent v2 Assay combined with Immunofluorescence - Integrated Co-Detection Workflow (ICW) Combinations*. 1–5.

Albanese, A., & Minciacchi, D. (1983). Organization of the ascending projections from the ventral tegmental area: A multiple fluorescent retrograde tracer study in the rat. *Journal of Comparative Neurology*, *216*(4), 406–420. https://doi.org/10.1002/cne.902160406

Alhassen, W., Kobayashi, Y., Su, J., Robbins, B., Nguyen, H., Myint, T., Yu, M., Nauli, S. M., Saito, Y., & Alachkar, A. (2021). Regulation of Brain Primary Cilia Length by MCH Signaling: Evidence from Pharmacological, Genetic, Optogenetic, and Chemogenic Manipulations. *Molecular Neurobiology*. https://doi.org/10.1007/s12035-021-02511-w

Bächner, D., Kreienkamp, H. J., Weise, C., Buck, F., & Richter, D. (1999). Identification of melanin concentrating hormone (MCH) as the natural ligand for the orphan somatostatin-like receptor 1 (SLC-1). *FEBS Letters*, *457*(3), 522–524. https://doi.org/10.1016/S0014-5793(99)01092-3

Barbano, M. F., Wang, H.-L., Zhang, S., Miranda-Barrientos, J., Estrin, D. J., Figueroa-González, A., Liu, B., Barker, D. J., & Morales, M. (2020). VTA glutamatergic neurons mediate innate defensive behaviors. *Neuron*, *107*, 368–382. https://doi.org/doi:10.1016/j.neuron.2020.04.024.

Bariselli, S., Glangetas, C., Tzanoulinou, S., & Bellone, C. (2016). Ventral tegmental area subcircuits process rewarding and aversive experiences. *Journal of Neurochemistry*, *139*(6), 1071–1080. https://doi.org/10.1111/jnc.13779

Barrot, M., Sesack, S. R., Georges, F., Pistis, M., Hong, S., & Jhou, T. C. (2012). Braking dopamine systems: A new GABA master structure for mesolimbic and nigrostriatal functions. *Journal of Neuroscience*, *32*(41), 14094–14101. https://doi.org/10.1523/JNEUROSCI.3370-12.2012

Berbari, N. F., Johnson, A. D., Lewis, J. S., Askwith, C. C., & Mykytyn, K. (2008). Identification of Ciliary Localization Sequences within the Third Intracellular Loop of G Protein-coupled Receptors. *Molecular Biology of the Cell*, *18*(April), 3250–3263.

Berbari, N. F., O'Connor, A. K., Haycraft, C. J., & Yoder, B. K. (2009). The Primary Cilium as a Complex Signaling Center. *Current Biology*, *19*(13), 1–21. https://doi.org/10.1016/j.cub.2009.05.025

Berridge, K. C. (2007). The debate over dopamine's role in reward: The case for incentive salience. *Psychopharmacology*, *191*(3), 391–431. https://doi.org/10.1007/s00213-006-0578-x

Bittencourt, J. C., Presse, F., Arias, C., Peto, C., Vaughan, J., Nahon, J. -L, Vale, W., & Sawchenko, P. E. (1992). The melanin-concentrating hormone system of the rat brain: An immuno- and hybridization histochemical characterization. *Journal of Comparative Neurology*, *319*(2), 218–245. https://doi.org/10.1002/cne.903190204

Bouarab, C., Thompson, B., & Polter, A. M. (2019). VTA GABA Neurons at the Interface of Stress and Reward. *Frontiers in Neural Circuits*, *13*(December), 1–12. https://doi.org/10.3389/fncir.2019.00078

Bromberg-Martin, E. S., Matsumoto, M., & Hikosaka, O. (2010). Dopamine in motivational control: rewarding, aversive, and alerting. *Neuron*, *68*(5), 815–834. https://doi.org/10.1016/j.neuron.2010.11.022.

Burdakov, D., Gerasimenko, O., & Verkhratsky, A. (2005). Physiological changes in glucose differentially modulate the excitability of hypothalamic melanin-concentrating hormone and orexin neurons in situ. *Journal of Neuroscience*, *25*(9), 2429–2433. https://doi.org/10.1523/JNEUROSCI.4925-04.2005

Cai, J., & Tong, Q. (2022). Anatomy and Function of Ventral Tegmental Area Glutamate Neurons. *Frontiers in Neural Circuits*, *16*(May). https://doi.org/10.3389/fncir.2022.867053

Chambers, J., Ames, R. S., Bergsma, D., Muir, A., Fitzgerald, L. R., Hervieu, G., Dytko, G. M., Foley, J. J., Martin, J., Liu, W. S., Park, J., Ellis, C., Ganguly, S., Konchar, S., Cluderay, J., Leslie, R., Wilson, S., & Sarau, H. M. (1999). Melanin-concentrating hormone is the cognate ligand for the orphan G- protein-coupled receptor SLC-1. *Nature*, *400*(6741), 261–265. https://doi.org/10.1038/22313

Chee, M. J., Hebert, A. J., Briançon, N., Flaherty, S. E., Pissios, P., & Maratos-Flier, E. (2019). Conditional deletion of melanin-concentrating hormone receptor 1 from GABAergic neurons increases locomotor activity. *Molecular Metabolism*, *29*(August), 114–123. https://doi.org/10.1016/j.molmet.2019.08.018

Chee, M. J. S., Arrigoni, E., & Maratos-Flier, E. (2015). Melanin-concentrating hormone neurons release glutamate for feedforward inhibition of the lateral septum. *Journal of Neuroscience*, *35*(8), 3644–3651. https://doi.org/10.1523/JNEUROSCI.4187-14.2015

Chee, M. J. S., Pissios, P., & Maratos-Flier, E. (2013). Neurochemical characterization of neurons expressing MCHR1 in mouse hypothalamus. *Journal of Comparative Neurology*, *521*(10), 2208–2234. https://doi.org/10.1002/cne.23273.Neurochemical

Chen, Y., Hu, C., Hsu, C. K., Zhang, Q., Bi, C., Asnicar, M., Hsiung, H. M., Fox, N., Slieker, L. J., Yang, D. D., Heiman, M. L., & Shi, Y. (2002). Targeted disruption of the melanin-concentrating hormone receptor-1 results in hyperphagia and resistance to diet-induced obesity. *Endocrinology*, *143*(7), 2469–2477. https://doi.org/10.1210/endo.143.7.8903

Cippitelli, A., Karlsson, C., Shaw, J. L., Thorsell, A., Gehlert, D. R., & Heilig, M. (2010). Suppression of alcohol self-administration and reinstatement of alcohol seeking by melanin-concentrating hormone receptor 1 (MCH1-R) antagonism in Wistar rats. *Psychopharmacology*, *211*(4), 367–375. https://doi.org/10.1007/s00213-010-1891-y

Clegg, D. J., Air, E. L., Benoit, S. C., Sakai, R. S., Seeley, R. J., & Woods, S. C. (2003). Intraventricular melanin-concentrating hormone stimulates water intake independent of food intake. *American Journal of Physiology - Regulatory Integrative and Comparative Physiology*, *284*(2 53-2), 494–499. https://doi.org/10.1152/ajpregu.00399.2002

Cohen, J. Y., Haesler, S., Vong, L., Lowell, B. B., & Uchida, N. (2012). Neuron-type-specific signals for reward and punishment in the ventral tegmental area. *Nature*, *482*(7383), 85–88. https://doi.org/10.1038/nature10754

Croizier, S., Franchi-Bernard, G., Colard, C., Poncet, F., la Roche, A., & Risold, P. Y. (2010). A comparative analysis shows morphofunctional differences between the rat and mouse melanin-concentrating hormone systems. *PLoS ONE*, *5*(11). https://doi.org/10.1371/journal.pone.0015471

Dahlstroem, A., & Fuxe, K. (1964). Evidence for the existence of monoamine-containing neurons in the central nervous system. I. demonstration of monoamines in the cell bodies of brain stem neurons. *Acta Physiologica Scandinavica.*, *Supplement*, 1–55.

Dal Bo, G., St.-Gelais, F., Danik, M., Williams, S., Cotton, M., & Trudeau, L. E. (2004). Dopamine neurons in culture express VGLUT2 explaining their capacity to release glutamate at synapses in addition to dopamine. *Journal of Neurochemistry*, *88*(6), 1398–1405. https://doi.org/10.1046/j.1471-4159.2003.02277.x

del Cid-Pellitero, E., & Jones, B. E. (2012). Immunohistochemical evidence for synaptic release of GABA from melanin-concentrating hormone containing varicosities in the locus coeruleus. *Neuroscience*, *223*, 269–276. https://doi.org/10.1016/j.neuroscience.2012.07.072

Della-Zuana, O., Presse, F., Ortola, C., Nahon, J. L., & Levens, N. (2002). Acute and chronic administration of melanin-concentrating hormone enhances food intake and body weight in Wistar and Sprague-Dawley rats. *International Journal of Obesity*, *26*(10), 1289–1295. https://doi.org/10.1038/sj.ijo.0802079

Diniz, G. B., Battagello, D. S., Klein, M. O., Bono, B. S. M., Ferreira, J. G. P., Motta-Teixeira, L. C., Duarte, J. C. G., Presse, F., Nahon, J. L., Adamantidis, A., Chee, M. J., Sita, L. V., & Bittencourt, J. C. (2020). Ciliary melanin-concentrating hormone receptor 1 (MCHR1) is widely distributed in the murine CNS in a sex-independent manner. *Journal of Neuroscience Research*, *98*(10), 2045–2071. https://doi.org/10.1002/jnr.24651

Diniz, G. B., & Bittencourt, J. C. (2017). The melanin-concentrating hormone as an integrative peptide driving motivated behaviors. *Frontiers in Systems Neuroscience*, *11*(May), 1–26. https://doi.org/10.3389/fnsys.2017.00032

Dobi, A., Margolis, E. B., Wang, H. L., Harvey, B. K., & Morales, M. (2010). Glutamatergic and nonglutamatergic neurons of the ventral tegmental area establish local synaptic contacts with dopaminergic and nondopaminergic neurons. *Journal of Neuroscience*, *30*(1), 218–229. https://doi.org/10.1523/JNEUROSCI.3884-09.2010

Domingos, A. I., Sordillo, A., Dietrich, M. O., Liu, Z. W., Tellez, L. A., Vaynshteyn, J., Ferreira, J. G., Ekstrand, M. I., Horvath, T. L., de Araujo, I. E., & Friedman, J. M. (2013). Hypothalamic melanin concentrating hormone neurons communicate the nutrient value of sugar. *ELife*, *2013*(2), 1–15. https://doi.org/10.7554/eLife.01462

Dong, H. (2008). *The Allen reference atlas: A digital color brain atlas of the C57BL/6J male mouse.* John Wiley & Sons.

Elias, C. F., Aschkenasi, C., Lee, C., Kelly, J., Ahima, R. S., Bjorbaek, C., Flier, J. S., Saper, C. B., & Elmquist, J. K. (1999). Leptin Differentially Regulates NPY and POMC Neurons Projecting to the Lateral Hypothalamic Area. *Neuron*, *23*, 775–786.

Elias, C. F., Saper, C. B., Maratos-Flier, E., Tritos, N. A., Lee, C., Kelly, J., Tatro, J. B., Huffman, G. E., Ollmann, M. M., Barsh, G. S., Sakurai, T., Yanagisawa, M., & Elmquist, J. K. (1998). Chemically defined projections linking the mediobasal hypothalamus and the lateral hypothalamic area. *Journal of Comparative Neurology*, *402*(4), 442–459. https://doi.org/10.1002/(SICI)1096-9861(19981228)402:4<442::AID-CNE2>3.0.CO;2-R

Eshel, N., Bukwich, M., Rao, V., Hemmelder, V., Tian, J., & Uchida, N. (2015). Arithmetic and local circuitry underlying dopamine prediction errors. *Nature*, *525*, 243–246. https://doi.org/doi:10.1038/nature14855

Faget, L., Osakada, F., Duan, J., Ressler, R., Johnson, A. B., Proudfoot, J. A., Yoo, J. H., Callaway, E. M., & Hnasko, T. S. (2016). Afferent Inputs to Neurotransmitter-Defined Cell Types in the Ventral Tegmental Area. *Cell Reports*, *15*(12), 2796–2808. https://doi.org/10.1016/j.celrep.2016.05.057

Georgescu, D., Sears, R. M., Hommel, J. D., Barrot, M., Bolaños, C. A., Marsh, D. J., Bednarek, M. A., Bibb, J. A., Maratos-Flier, E., Nestler, E. J., & DiLeone, R. J. (2005). The hypothalamic neuropeptide melanin-concentrating hormone acts in the nucleus accumbens to modulate feeding behavior and forced-swim performance. *Journal of Neuroscience*, *25*(11), 2933–2940. https://doi.org/10.1523/JNEUROSCI.1714-04.2005

Gomori, A., Ishihara, A., Ito, M., Matsushita, H., Ito, M., Mashiko, S., Iwaasa, H., Matsuda, M., Bednarek, M. A., Qian, S., MacNeil, D. J., & Kanatani, A. (2007). Blockade of MCH1 receptor signalling ameliorates obesity and related hepatic steatosis in ovariectomized mice. *British Journal of Pharmacology*, *151*(6), 900–908. https://doi.org/10.1038/sj.bjp.0707292

Gomori, Akira, Ishihara, A., Ito, M., Mashiko, S., Matsushita, H., Yumoto, M., Ito, M., Tanaka, T., Tokita, S., Moriya, M., Iwaasa, H., & Kanatani, A. (2002). Chronic intracerebroventricular infusion of MCH causes obesity in mice. *American Journal of Physiology - Endocrinology and Metabolism*, *284*(3 47-3), 583–588. https://doi.org/10.1152/ajpendo.00350.2002

Grossman, S. P., Dacey, D., Halaris, A. E., Collier, T., & Routtenberg, A. (1978). Aphagia and adipsia after preferential destruction of nerve cell bodies in hypothalamus. *Science*, *202*, 537–539.

Guan, Y., Xiao, C., Krnjević, K., Xie, G., Zuo, W., & Ye, J.-H. (2012). GABAergic Actions Mediate Opposite Ethanol Effects on Dopaminergic Neurons in the Anterior and Posterior Ventral Tegmental Area. *Journal of Pharmacology and Experimental Therapeutics*, *341*(1), 33–42. https://doi.org/10.1124/jpet.111.187963

Gunaydin, L. A., Grosenick, L., Finkelstein, J. C., Kauvar, I. V., Fenno, L. E., Adhikari, A., Lammel, S., Mirzabekov, J. J., Airan, R. D., Zalocusky, K. A., Tye, K. M., Anikeeva, P., Malenka, R. C., & Deisseroth, K. (2014). Natural neural projection dynamics underlying social behavior. *Cell*, *157*(7), 1535–1551. https://doi.org/10.1016/j.cell.2014.05.017

Hawes, B. E., Erin, K. I. L., Green, B., O'Neill, K. I. M., Fried, S., & Graziano, M. P. (2000). The melanin-concentrating hormone receptor couples to multiple G proteins to activate diverse intracellular signaling pathways. *Endocrinology*, *141*(12), 4524–4532. https://doi.org/10.1210/endo.141.12.7833

Hervieu, G. J., Cluderay, J. E., Harrison, D., Meakin, J., Maycox, P., Nasir, S., & Leslie, R. A. (2000). The distribution of the mRNA and protein products of the melanin-concentrating hormone (MCH) receptor gene, slc-1, in the central nervous system of the ratt. *European Journal of Neuroscience*, *12*(4), 1194–1216. https://doi.org/10.1046/j.1460-9568.2000.00008.x

Ito, M., Ishihara, A., Gomori, A., Matsushita, H., Ito, M., Metzger, J. M., Marsh, D. J., Haga, Y., Iwaasa, H., Tokita, S., Takenaga, N., Sato, N., MacNeil, D. J., Moriya, M., & Kanatani, A. (2010). Mechanism of the anti-obesity effects induced by a novel Melanin-concentrating hormone 1-receptor antagonist in mice. *British Journal of Pharmacology*, *159*(2), 374–383. https://doi.org/10.1111/j.1476-5381.2009.00536.x

Jasso, K. R., Kamba, T. K., Zimmerman, A. D., Bansal, R., Engle, S. E., Everett, T., Wu, C. H., Kulaga, H., Reed, R. R., Berbari, N. F., & McIntyre, J. C. (2021). An N-terminal fusion allele to study melanin concentrating hormone receptor 1. *Genesis*, *59*(7–8), 1–12. https://doi.org/10.1002/dvg.23438

Jego, S., Glasgow, S. D., Herrera, C. G., Ekstrand, M., Reed, S. J., Boyce, R., Friedman, J., Burdakov, D., & Adamantidis, A. R. (2013). Optogenetic identification of a rapid eye movement sleep modulatory circuit in the hypothalamus. *Nature Neuroscience*, *16*(11), 1637–1643. https://doi.org/10.1038/nn.3522

Jhou, T. C. (2021). The rostromedial tegmental (RMTg) “brake” on dopamine and behavior: A decade of progress but also much unfinished work. *Neuropharmacology*, *198*(August), 108763. https://doi.org/10.1016/j.neuropharm.2021.108763

Jhou, T., Fields, H., Baxter, M., & Saper, C. (2009). The rostromedial tegmental nucleus (RMTg), a major GABAergic afferent to midbrain dopamine neurons, selectively encodes aversive stimuli and promotes behavioral inhibition. *Neuron*, *61*(5), 786–800. https://doi.org/10.1016/j.neuron.2009.02.001.The

Karlsson, C., Rehman, F., Damdazic, R., Atkins, A. L., Schank, J. R., Gehlert, D. R., Steensland, P., Thorsell, A., & Heilig, M. (2016). The melanin-concentrating hormone-1 receptor modulates alcohol-induced reward and DARPP-32 phosphorylation. *Psychopharmacology*, *233*(12), 2355–2363. https://doi.org/10.1007/s00213-016-4285-y

Karlsson, C., Zook, M., Ciccocioppo, R., Gehlert, D. R., Thorsell, A., Heilig, M., & Cippitelli, A. (2012). Melanin-concentrating hormone receptor 1 (MCH1-R) antagonism: Reduced appetite for calories and suppression of addictive-like behaviors. *Pharmacology Biochemistry and Behavior*, *102*(3), 400–406. https://doi.org/10.1016/j.pbb.2012.06.010

Kempadoo, K. A., Tourino, C., Cho, S. L., Magnani, F., Leinninger, G. M., Stuber, G. D., Zhang, F., Myers, M. G., Deisseroth, K., de Lecea, L., & Bonci, A. (2013). Hypothalamic neurotensin projections promote reward by enhancing glutamate transmission in the VTA. *Journal of Neuroscience*, *33*(18), 7618–7626. https://doi.org/10.1523/JNEUROSCI.2588-12.2013

Kiernan, J. (2001). Classification and naming of dyes, stains and fluorochromes. *Biotechnic & Histochemistry*, *76*(5–6), 261–278. https://doi.org/10.1080/bih.76.5-6.261.278

Kobayashi, Y., Okada, T., Miki, D., Sekino, Y., Koganezawa, N., Shirao, T., Diniz, G. B., & Saito, Y. (2021). Properties of primary cilia in melanin-concentrating hormone receptor 1-bearing hippocampal neurons in vivo and in vitro. *Neurochemistry International*, *142*(May 2020), 104902. https://doi.org/10.1016/j.neuint.2020.104902

Kokkotou, E. G., Tritos, N. A., Mastaitis, J. W., Slieker, L., & Maratos-Flier, E. (2001). Melanin-concentrating hormone receptor is a target of leptin action in the mouse brain. *Endocrinology*, *142*(2), 680–686. https://doi.org/10.1210/endo.142.2.7981

Kokkotou, E., Jeon, J. Y., Wang, X., Marino, F. E., Carlson, M., Trombly, D. J., & Maratos-Flier, E. (2005). Mice with MCH ablation resist diet-induced obesity through strain-specific mechanisms. *American Journal of Physiology - Regulatory Integrative and Comparative Physiology*, *289*(1 58-1), 117–124. https://doi.org/10.1152/ajpregu.00861.2004

Kong, D., Vong, L., Parton, L. E., Ye, C., Tong, Q., Choi, B., Brüning, J. C., & Lowell, B. B. (2010). Glucose Stimulation of Hypothalamic MCH Neurons Involves KATP Channels, is Modulated by UCP2, and Regulates Peripheral Glucose Homeostasis. *Cell Metabolism*, *2*(15), 545–552. https://doi.org/10.1016/j.cmet.2010.09.013.

Korotkova, T. M., Sergeeva, O. A., Eriksson, K. S., Haas, H. L., & Brown, R. E. (2003). Excitation of ventral tegmental area dopaminergic and nondopaminergic neurons by orexins/hypocretins. *Journal of Neuroscience*, *23*(1), 7–11. https://doi.org/10.1523/jneurosci.23-01-00007.2003

Krashes, M. J., Shah, B. P., Madara, J. C., Olson, D. P., Strochlic, D. E., Garfield, A. S., Vong, L., Pei, H., Watabe-Uchida, M., Uchida, N., Liberles, S. D., & Lowell, B. B. (2014). An excitatory paraventricular nucleus to AgRP neuron circuit that drives hunger. *Nature*, *507*(7491), 238–242. https://doi.org/10.1038/nature12956.A

Lahti, L., Haugas, M., Tikker, L., Airavaara, M., Voutilainen, M. H., Anttila, J., Kumar, S., Inkinen, C., Salminen, M., & Partanen, J. (2016). Differentiation and molecular heterogeneity of inhibitory and excitatory neurons associated with midbrain dopaminergic nuclei. *Development (Cambridge)*, *143*(3), 516–529. https://doi.org/10.1242/dev.129957

Lecca, S., Melis, M., Luchicchi, A., Muntoni, A. L., & Pistis, M. (2012). Inhibitory inputs from rostromedial tegmental neurons regulate spontaneous activity of midbrain dopamine cells and their responses to drugs of abuse. *Neuropsychopharmacology*, *37*(5), 1164–1176. https://doi.org/10.1038/npp.2011.302

Lembo, P. M. C., Grazzini, E., Cao, J., Hubatsch, D. A., Pelletier, M., Hoffert, C., St-Onge, S., Pou, C., Labrecque, J., Groblewski, T., O'Donnell, D., Payza, K., Ahmad, S., & Walker, P. (1999). The receptor for the orexigenic peptide melanin-concentrating hormone is a G-protein-coupled receptor. *Nature Cell Biology*, *1*(5), 267–271. https://doi.org/10.1038/12978

Ludwig, D. S., Tritos, N. A., Mastaitis, J. W., Kulkarni, R., Kokkotou, E., Elmquist, J., Lowell, B., Flier, J. S., & Maratos-Flier, E. (2001). Melanin-concentrating hormone overexpression in transgenic mice leads to obesity and insulin resistance. *Journal of Clinical Investigation*, *107*(3), 379–386. https://doi.org/10.1172/JCI10660

Margolis, E. B., Lock, H., Hjelmstad, G. O., & Fields, H. L. (2006). The ventral tegmental area revisited: Is there an electrophysiological marker for dopaminergic neurons? *Journal of Physiology*, *577*(3), 907–924. https://doi.org/10.1113/jphysiol.2006.117069

Marsh, D. J., Weingarth, D. T., Novi, D. E., Chen, H. Y., Trumbauer, M. E., Chen, A. S., Guan, X. M., Jiang, M. M., Feng, Y., Camacho, R. E., Shen, Z., Frazier, E. G., Yu, H., Metzger, J. M., Kuca, S. J., Shearman, L. P., Gopal-Truter, S., MacNeil, D. J., Strack, A. M., … Qian, S. (2002). Melanin-concentrating hormone 1 receptor-deficient mice are lean, hyperactive, and hyperphagic and have altered metabolism. *Proceedings of the National Academy of Sciences of the United States of America*, *99*(5), 3240–3245. https://doi.org/10.1073/pnas.052706899

Mashiko, S., Ishihara, A., Gomori, A., Moriya, R., Ito, M., Iwaasa, H., Matsuda, M., Feng, Y., Shen, Z., Marsh, D. J., Bednarek, M. A., MacNeil, D. J., & Kanatani, A. (2005). Antiobesity effect of a melanin-concentrating hormone 1 receptor antagonist in diet-induced obese mice. *Endocrinology*, *146*(7), 3080–3086. https://doi.org/10.1210/en.2004-1150

Mickelsen, L. E., Kolling, F. W., Chimileski, B. R., Fujita, A., Norris, C., Chen, K., Nelson, C. E., & Jackson, A. C. (2017). Neurochemical heterogeneity among lateral hypothalamic hypocretin/orexin and melanin-concentrating hormone neurons identified through single-cell gene expression analysis. *ENeuro*, *4*(5). https://doi.org/10.1523/ENEURO.0013-17.2017

Miranda-Barrientos, J., Chambers, I., Mongia, S., Liu, B., Wang, H. L., Mateo-Semidey, G. E., Margolis, E. B., Zhang, S., & Morales, M. (2021). Ventral tegmental area GABA, glutamate, and glutamate-GABA neurons are heterogeneous in their electrophysiological and pharmacological properties. *European Journal of Neuroscience*, *54*(1), 4061–4084. https://doi.org/10.1111/ejn.15156

Morales, M., & Root, D. H. (2014). Glutamate neurons within the midbrain dopamine regions. *Neuroscience*, *282*, 60–68. https://doi.org/10.1016/j.neuroscience.2014.05.032

Morales, Marisela, & Margolis, E. B. (2017). Ventral tegmental area: Cellular heterogeneity, connectivity and behaviour. *Nature Reviews Neuroscience*, *18*(2), 73–85. https://doi.org/10.1038/nrn.2016.165

Mul, J. D., la Fleur, S. E., Toonen, P. W., Afrasiab-Middelman, A., Binnekade, R., Schetters, D., Verheij, M. M. M., Sears, R. M., Homberg, J. R., Schoffelmeer, A. N. M., Adan, R. A. H., DiLeone, R. J., de Vries, T. J., & Cuppen, E. (2011). Chronic loss of melanin-concentrating hormone affects motivational aspects of feeding in the rat. *PLoS ONE*, *6*(5). https://doi.org/10.1371/journal.pone.0019600

Negishi, K., Payant, M. A., Schumacker, K. S., Wittmann, G., Butler, R. M., Lechan, R. M., Steinbusch, H. W. M., Khan, A. M., & Chee, M. J. (2020). Distributions of hypothalamic neuron populations coexpressing tyrosine hydroxylase and the vesicular GABA transporter in the mouse. *Journal of Comparative Neurology*, *528*(11), 1833–1855. https://doi.org/10.1002/cne.24857

Nieh, E. H., Matthews, G. A., Allsop, S. A., Presbrey, K. N., Leppla, C. A., Wichmann, R., Neve, R., Wildes, C. P., & Kay, M. (2015). Decoding Neural Circuits that Control Compulsive Sucrose- Seeking. *Cell*, *160*(3), 528–541. https://doi.org/10.1016/j.cell.2015.01.003.Decoding

Nieh, E. H., Vander Weele, C. M., Matthews, G. A., Presbrey, K. N., Wichmann, R., Leppla, C. A., Izadmehr, E. M., & Tye, K. M. (2016). Inhibitory Input from the Lateral Hypothalamus to the Ventral Tegmental Area Disinhibits Dopamine Neurons and Promotes Behavioral Activation. *Neuron*, *90*(6), 1286–1298. https://doi.org/10.1016/j.neuron.2016.04.035

Noble, E. E., Hahn, J. D., Konanur, V. R., Hsu, T. M., Page, S. J., Cortella, A. M., Liu, C. M., Song, M. Y., Suarez, A. N., Caroline, C., Rider, D., Clarke, J. E., Darvas, M., Appleyard, S. M., & Kanoski, S. E. (2018). Control of feeding behavior by cerebral ventricular volume transmission of melanin-concentrating hormone. *Cell Metabolism*, *28*(1), 55–68. https://doi.org/10.1016/j.cmet.2018.05.001.Control

Pachoud, B., Adamantidis, A., Ravassard, P., Luppi, P. H., Grisar, T., Lakaye, B., & Salin, P. A. (2010). Major impairments of glutamatergic transmission and long-term synaptic plasticity in the hippocampus of mice lacking the melanin-concentrating hormone receptor-1. *Journal of Neurophysiology*, *104*(3), 1417–1425. https://doi.org/10.1152/jn.01052.2009

Pissios, P., Frank, L., Kennedy, A. R., Porter, D. R., Marino, F. E., Liu, F. F., Pothos, E. N., & Maratos-Flier, E. (2008). Dysregulation of the Mesolimbic Dopamine System and Reward in MCH-/- Mice. *Biological Psychiatry*, *64*(3), 184–191. https://doi.org/10.1016/j.biopsych.2007.12.011

Pissios, P., Trombly, D. J., Tzameli, I., & Maratos-Flier, E. (2003). Melanin-concentrating hormone receptor 1 activates extracellular signal-regulated kinase and synergizes with Gs-coupled pathways. *Endocrinology*, *144*(8), 3514–3523. https://doi.org/10.1210/en.2002-0004

Polter, A. M., Barcomb, K., Tsuda, A. C., & Kauer, J. A. (2018). Synaptic function and plasticity in identified inhibitory inputs onto VTA dopamine neurons Abigail. *Eur J Neurosci*, *47*(10), 1208–1218. https://doi.org/10.1111/ejn.13879.

Qu, D., Ludwig, D. S., Gammeltoftt, S., Piper, M., Pelleymountert, M. A., Cullent, M. J., Mathes, W. F., Przypek, J., Kanarek, R., & Ii, E. M. (1996). A role for melanin-concentrating hormone in the central regulation of feeding behaviour. *Nature*, *380*(March), 243–247.

Root, D. H., Barker, D. J., Estrin, D. J., Miranda-Barrientos, J. A., Liu, B., Zhang, S., Wang, H. L., Vautier, F., Ramakrishnan, C., Kim, Y. S., Fenno, L., Deisseroth, K., & Morales, M. (2020). Distinct Signaling by Ventral Tegmental Area Glutamate, GABA, and Combinatorial Glutamate-GABA Neurons in Motivated Behavior. *Cell Reports*, *32*(9), 108094. https://doi.org/10.1016/j.celrep.2020.108094

Root, D. H., Mejias-Aponte, C. A., Qi, J., & Morales, M. (2014). Role of glutamatergic projections from ventral tegmental area to lateral Habenula in aversive conditioning. *Journal of Neuroscience*, *34*(42), 13906–13910. https://doi.org/10.1523/JNEUROSCI.2029-14.2014

Root, D. H., Mejias-Aponte, C. A., Zhang, S., Wang, H. L., Hoffman, A. F., Lupica, C. R., & Morales, M. (2014). Single rodent mesohabenular axons release glutamate and GABA. *Nature Neuroscience*, *17*(11), 1543–1551. https://doi.org/10.1038/nn.3823

Root, D. H., Zhang, S., Barker, D. J., Miranda-Barrientos, J., Liu, B., Wang, H. L., & Morales, M. (2018). Selective Brain Distribution and Distinctive Synaptic Architecture of Dual Glutamatergic-GABAergic Neurons. *Cell Reports*, *23*(12), 3465–3479. https://doi.org/10.1016/j.celrep.2018.05.063

Rossi, M., Choi, S. J., O'Shea, D., Miyoshi, T., Ghatei, M. A., & Bloom, S. R. (1997). Melanin-concentrating hormone acutely stimulates feeding, but chronic administration has no effect on body weight. *Endocrinology*, *138*(1), 351–355. https://doi.org/10.1210/endo.138.1.4887

Saito, Y., Cheng, M., Leslie, F. M., & Civelli, O. (2001). Expression of the melanin-concentrating hormone (MCH) receptor mRNA in the rat brain. *Journal of Comparative Neurology*, *435*(1), 26–40. https://doi.org/10.1002/cne.1191

Saito, Y., Nothacker, H., Wang, Z., Lin, S. H. S., Leslie, F., & Civelli, O. (1999). Molecular characterization of the melanin-concentrating- hormone receptor. *Nature*, *400*(July), 265–269.

Salamone, J. D., & Correa, M. (2012). THE MYSTERIOUS MOTIVATIONAL FUNCTIONS OF MESOLIMBIC DOPAMINE. *Neuron*, *76*(3), 470–485. https://doi.org/10.1016/j.neuron.2012.10.021.

Sanchez-Catalan, M. J., Kaufling, J., Georges, F., Veinante, P., & Barrot, M. (2014). The antero-posterior heterogeneity of the ventral tegmental area. *Neuroscience*, *282*, 198–216. https://doi.org/10.1016/j.neuroscience.2014.09.025

Saper, C. B., Chou, T. C., & Elmquist, J. K. (2002). The Need to Feed: Homeostatic and Hedonic Control of Eating. *Neuron*, *36*, 199–211.

Schneeberger, M., Tan, K., Nectow, A. R., Parolari, L., Caglar, C., Azevedo, E., Li, Z., Domingos, A., & Friedman, J. M. (2018). Functional analysis reveals differential effects of glutamate and MCH neuropeptide in MCH neurons. *Molecular Metabolism*, *13*(May), 83–89. https://doi.org/10.1016/j.molmet.2018.05.001

Schultz, W., Dayan, P., & Montague, P. R. (1997). A neural substrate of prediction and reward. *Science*, *275*(5306), 1593–1599. https://doi.org/10.1126/science.275.5306.1593

Schultz, Wolfram. (2002). Getting formal with dopamine and reward. *Neuron*, *36*(2), 241–263. https://doi.org/10.1016/S0896-6273(02)00967-4

Segal-Lieberman, G., Bradley, R. L., Kokkotou, E., Carlson, M., Trombly, D. J., Wang, X., Bates, S., Myers, M. G., Flier, J. S., & Maratos-Flier, E. (2003). Melanin-concentrating hormone is a critical mediator of the leptin-deficient phenotype. *Proceedings of the National Academy of Sciences of the United States of America*, *100*(17), 10085–10090. https://doi.org/10.1073/pnas.1633636100

Shearman, L. P., Camacho, R. E., Stribling, D. S., Zhou, D., Bednarek, M. A., Hreniuk, D. L., Feighner, S. D., Tan, C. P., Howard, A. D., Van Der Ploeg, L. H. T., MacIntyre, D. E., Hickey, G. J., & Strack, A. M. (2003). Chronic MCH-1 receptor modulation alters appetite, body weight and adiposity in rats. *European Journal of Pharmacology*, *475*(1–3), 37–47. https://doi.org/10.1016/S0014-2999(03)02146-0

Shimada, M., Tritos, N. A., Lowell, B. B., Flier, J. S., & Maratos-Flier, E. (1998). Mice lacking melanin- concentrating hormone are hypophagic and lean. *Nature*, *396*(December), 3–7.

Simmons, D. N. V., Petko, A. K., & Paladini, C. A. (2017). Differential expression of long-term potentiation among identified inhibitory inputs to dopamine neurons. *Journal of Neurophysiology*, *118*(4), 1998–2008. https://doi.org/10.1152/jn.00270.2017

Stamatakis, A. M., Jennings, J. H., Ung, R. L., Blair, G. A., Weinberg, J., Neve, R. L., Boyce, F., Mattis, J., Deisseroth, K., & Stuber, G. D. (2013). A unique population of ventral tegmental area neurons inhibits the lateral habenula to promote reward. *Neuron*, *80*(4), 1–23. https://doi.org/10.1016/j.neuron.2013.08.023.A

Stricker, E. M., Swerdloff, A. F., & Zigmond, M. J. (1978). Intrahypothalamic injections of kainic acid produce feeding and drinking deficits in rats. *Brain Research*, *158*(2), 470–473. https://doi.org/10.1016/0006-8993(78)90692-3

Stuber, G. D., Hnasko, T. S., Britt, J. P., Edwards, R. H., & Bonci, A. (2010). Dopaminergic terminals in the nucleus accumbens but not the dorsal striatum corelease glutamate. *Journal of Neuroscience*, *30*(24), 8229–8233. https://doi.org/10.1523/JNEUROSCI.1754-10.2010

Sulzer, D., Joyce, M. P., Lin, L., Geldwert, D., Haber, S. N., Hattori, T., & Rayport, S. (1998). Dopamine neurons make glutamatergic synapses in vitro. *Journal of Neuroscience*, *18*(12), 4588–4602. https://doi.org/10.1523/jneurosci.18-12-04588.1998

Tan, C. P., Sano, H., Iwaasa, H., Pan, J., Sailer, A. W., Hreniuk, D. L., Feighner, S. D., Palyha, O. C., Pong, S. S., Figueroa, D. J., Austin, C. P., Jiang, M. M., Yu, H., Ito, J., Ito, M., Ito, M., Guan, X. M., MacNeil, D. J., Kanatani, A., … Howard, A. D. (2002). Melanin-concentrating hormone receptor subtypes 1 and 2: Species-specific gene expression. *Genomics*, *79*(6), 785–792. https://doi.org/10.1006/geno.2002.6771

Tan, K. R., Yvon, C., Turiault, M., Mirzabekov, J. J., Doehner, J., Labouèbe, G., Deisseroth, K., Tye, K. M., & Lüscher, C. (2012). GABA Neurons of the VTA Drive Conditioned Place Aversion. *Neuron*, *73*(6), 1173–1183. https://doi.org/10.1016/j.neuron.2012.02.015

Tecuapetla, F., Patel, J. C., Xenias, H., English, D., Tadros, I., Shah, F., Berlin, J., Deisseroth, K., Rice, M. E., Tepper, J. M., & Koos, T. (2010). Glutamatergic signaling by mesolimbic dopamine neurons in the nucleus accumbens. *Journal of Neuroscience*, *30*(20), 7105–7110. https://doi.org/10.1523/JNEUROSCI.0265-10.2010

Tepper, J. M., & Lee, C. R. (2007). GABAergic control of substantia nigra dopaminergic neurons. *Progress in Brain Research*, *160*(06), 189–208. https://doi.org/10.1016/S0079-6123(06)60011-3

Tian, J., Huang, R., Cohen, J. Y., Osakada, F., Kobak, D., Machens, C. K., Callaway, E. M., Uchida, N., & Watabe-Uchida, M. (2016). Distributed and Mixed Information in Monosynaptic Inputs to Dopamine Neurons. *Neuron*, *91*(6), 1374–1389. https://doi.org/10.1016/j.neuron.2016.08.018

Ting, J. T., Lee, B. R., Chong, P., Soler-Llavina, G., Cobbs, C., Koch, C., Zeng, H., & Lein, E. (2018). Preparation of Acute Brain Slices Using an Optimized N-Methyl-D-glucamine Protective Recovery Method. *Journal of Visualized Experiments : JoVE*, *132*, 1–13. https://doi.org/10.3791/53825

Tritos, N. A., Vicent, D., Gillette, J., Ludwig, D. S., Flier, E. S., & Maratos-Flier, E. (1998). Functional interactions between melanin-concentrating hormone, neuropeptide Y, and anorectic neuropeptides in the rat hypothalamus. *Diabetes*, *47*(11), 1687–1692. https://doi.org/10.2337/diabetes.47.11.1687

Tritsch, N. X., Ding, J. B., & Sabatini, B. L. (2012). Dopaminergic neurons inhibit striatal output via non-canonical release of GABA. *Nature*, *490*, 262–266. https://doi.org/doi:10.1038/nature11466

Van Zessen, R., Phillips, J. L., Budygin, E. A., & Stuber, G. D. (2012). Activation of VTA GABA Neurons Disrupts Reward Consumption. *Neuron*, *73*(6), 1184–1194. https://doi.org/10.1016/j.neuron.2012.02.016

Volkow, N. D., & Wise, R. A. (2005). How can drug addiction help us understand obesity? *Nature Neuroscience*, *8*(5), 555–560. https://doi.org/10.1038/nn1452

Wang, H. L., Qi, J., Zhang, S., Wang, H., & Morales, M. (2015). Rewarding effects of optical stimulation of ventral tegmental area glutamatergic neurons. *Journal of Neuroscience*, *35*(48), 15948–15954. https://doi.org/10.1523/JNEUROSCI.3428-15.2015

Wheatley, D. N. (2008). Nanobiology of the Primary Cilium—Paradigm of a Multifunctional Nanomachine Complex. *Methods in Cell Biology*, *90*, 139–156.

Wise, R. A. (2004). Dopamine, learning and motivation. *Nature Reviews Neuroscience*, *5*(6), 483–494. https://doi.org/10.1038/nrn1406

Wise, R. A. (2006). Role of brain dopamine in food reward and reinforcement. *Philosophical Transactions of the Royal Society B: Biological Sciences*, *361*(1471), 1149–1158. https://doi.org/10.1098/rstb.2006.1854

Wu, M., Dumalska, I., Morozova, E., Van Den Pol, A., & Alreja, M. (2009). Melanin-concentrating hormone directly inhibits GnRH neurons and blocks kisspeptin activation, linking energy balance to reproduction. *Proceedings of the National Academy of Sciences of the United States of America*, *106*(40), 17217–17222. https://doi.org/10.1073/pnas.0908200106

Yamaguchi, T., Sheen, W., & Morales, M. (2007). Glutamatergic neurons are present in the rat ventral tegmental area. *Eur J Neurosci*, *25*(1), 106–118. https://doi.org/doi:10.1111/j.1460-9568.2006.05263.x.

Yamaguchi, T., Wang, H. L., Li, X., Ng, T. H., & Morales, M. (2011). Mesocorticolimbic glutamatergic pathway. *Journal of Neuroscience*, *31*(23), 8476–8490. https://doi.org/10.1523/JNEUROSCI.1598-11.2011

Yoo, J. H., Zell, V., Gutierrez-Reed, N., Wu, J., Ressler, R., Shenasa, M. A., Johnson, A. B., Fife, K. H., Faget, L., & Hnasko, T. S. (2016). Ventral tegmental area glutamate neurons co-release GABA and promote positive reinforcement. *Nature Communications*, *7*(May), 1–13. https://doi.org/10.1038/ncomms13697

You, Z. B., Chen, Y. Q., & Wise, R. A. (2001). Dopamine and glutamate release in the nucleus accumbens and ventral tegmental area of rat following lateral hypothalamic self-stimulation. *Neuroscience*, *107*(4), 629–639. https://doi.org/10.1016/S0306-4522(01)00379-7

Zell, V., Steinkellner, T., Hollon, N. G., Warlow, S. M., Souter, E., Faget, L., Hunker, A. C., Jin, X., Zweifel, L. S., & Hnasko, T. S. (2020). VTA Glutamate Neuron Activity Drives Positive Reinforcement Absent Dopamine Co-release. *Neuron*, *107*(5), 864-873.e4. https://doi.org/10.1016/j.neuron.2020.06.011